12-1-2017

Miocene-Pliocene(?) Folds, Normal Faults and the Left-Lateral Buckhorn Fault with Regional Implications, Pahranagat Shear Zone, Nevada

Thomas Godfrey Price
University of Nevada, Las Vegas, osalith@gmail.com

MIOCENE-PLIOCENE(?) FOLDS, NORMAL FAULTS AND THE LEFT-LATERAL

BUCKHORN FAULT WITH REGIONAL IMPLICATIONS, PAHRANAGAT SHEAR ZONE,

NEVADA

By

Thomas G. Price

Bachelor of Science - Geology
University of Nevada Las Vegas
2013

A thesis submitted in partial fulfillment of the requirements for the

Master of Science – Geoscience

Department of Geoscience
College of Sciences
The Graduate College

University of Nevada, Las Vegas
December 2017

Thesis Approval

The Graduate College
The University of Nevada, Las Vegas

November 16, 2017

This thesis prepared by

Thomas G. Price

entitled

Miocene-Pliocene(?) Folds, Normal Faults and the Left-Lateral Buckhorn Fault with Regional Implications, Pahranagat Shear Zone, Nevada

is approved in partial fulfillment of the requirements for the degree of

Master of Science – Geoscience
Department of Geoscience

Wanda J. Taylor, Ph.D.
Examination Committee Chair

Arya Udry, Ph.D.
Examination Committee Member

Rodney Metcalf, Ph.D.
Examination Committee Member

Barbara Luke, Ph.D.
Graduate College Faculty Representative

Kathryn Hausbeck Korgan, Ph.D.
Graduate College Interim Dean

ABSTRACT

MIOCENE-PLIOCENE(?) FOLDS, NORMAL FAULTS AND THE LEFT-LATERAL BUCKHORN FAULT WITH REGIONAL IMPLICATIONS, PAHRANAGAT SHEAR ZONE, NEVADA

By

Thomas G. Price

Dr. Wanda J. Taylor, Examination Committee Chair

Professor of Geoscience

University of Nevada, Las Vegas

Strike-slip faults play an important role in the development and evolution of extensional regimes including in the intraplate extension in the Basin and Range province. The Basin and Range province is divided into the Northwestern, Northern, Central and Southern Basin and Range subprovinces. The boundary zone between the Northern and Central subprovinces is marked by several left-lateral fault zones, including the Pahranagat Shear Zone (PSZ), Caliente-Enterprise Zone and Rock Valley Fault Zone. The PSZ has a close spatial and kinematic relationship with the left-lateral Caliente-Enterprise Zone, which lies to the NE, and a slightly more distal relationship to the left-lateral Rock Valley Fault Zone off to the southwest. Understanding the internal deformation within these left-lateral zones is fundamental to understanding how these zones, in part or as a whole, accommodate deformation and interact with other structures. The PSZ consists of three ENE-striking left-lateral strike-slip faults: the Arrowhead Mine Fault, Buckhorn Fault (BF), and Maynard Lake

Fault, from north to south, respectively, with intervening normal to oblique slip faults and folds. Understanding the internal deformation is critical to understanding the PSZ as a whole, and thus, development of the sub-province boundary.

The BF, the largest structure internal to the PSZ, along with surrounding structures provides insight into the internal deformation history of the PSZ. Important surrounding structures include the Buckhorn Syncline and Anticline, which are located between the Arrowhead Mine Fault and the BF. Both of these structures formed from stresses internal to the PSZ. This study focuses on formation of strike-slip faults, timing of deformation, kinematic history, and geometry of structures using data from a new 1:12,000 scale map of the western BF and a new ^{40}Ar/^{39}Ar date.

Exposed structures near the BF display three ages of deformation: (1) an episode of early-Miocene normal faulting between 22.56 and 18.51 Ma, (2) mid-Miocene normal faulting between 18.51 Ma and 15.3 Ma, and (3) faulting and folding after deposition of the Kane Wash Tuff at15.3 Ma. The 15.3 Ma age was acquired from ^{40}Ar/^{39}Ar dating of sanidine crystals from the Kane Wash Tuff, subunit 3. The third deformation is the best preserved and exposed in the area. In addition, paleohills can be identified by a buttress unconformity between the Paleozoic strata and Tertiary ash-flow tuffs. Retrodeforming these paleohills by removing the three episodes of post 22.56 Ma deformations steepens the dip of bedding in the hills to >50° before deposition of the tuffs. The paleohill located just south of the BF is relatively internally undeformed and is here suggested to belong to the footwall of the Gass Peak Thrust, which is a part of the ~Cretaceous Sevier fold-and-thrust belt.

Overall, the boundary zone between the NBR and CBR is defined by a series of left-lateral zones including the PSZ. The folds and faults define a zone of3D (triaxial strain) within the

PSZ. The PSZ acts as part of the modern, and developing, transfer zone between the Eastern

California Shear Zone and/or Walker Lane Belt and the Wasatch Fault Zone/Intermountain

Seismic Belt.

AKNOWLEDGEMENTS

TABLE OF CONTENTS

LIST OF FIGURES

INTRODUCTION

The Northern Basin and Range (NBR) and Central Basin and Range (CBR) sub-provinces of the Basin and Range province in the western United States have distinct differences in basin elevations, timing of the onset of extension, and pattern of volcanism. Average basin elevations between the NBR and CBR are separated by 600 m with the NBR basins having the higher average elevation of 1250 m. Extension began in the NBR around 35 Ma and extension continued into the Miocene (Sonder and Jones, 1999) followed by Quaternary extension. Whereas, the onset of extension in the CBR is around 16-18 Ma in the east and younger in the center, ~12-14 Ma (Umhoefer et al., 2010; Bidgoli et al., 2015; Lamb et al., 2015). The NBR experienced volcanism which began in the north and progressed south or southwest to the boundary between the NBR and CBR (Rau and Forsyth, 2011). The CBR underwent little to no volcanism, although magmatism may have occurred at depth (Sonder and Jones, 1999). The boundary zone is marked by two caldera complexes, strike-slip fault zones, and Bouguer gravity anomalies (Fig. 1 and 2). This collection of features leads to the question, "How did the boundary between the sub-provinces develop throughout the Cenozoic?"

The NE-striking Pahranagat shear zone (PSZ) and E-W orientated Caliente-Enterprise Zone are left-lateral slip systems along the NBR-CBR boundary that extend westward from the Wasatch Fault Zone and Intermountain Seismic Belt to the Sheep Range detachment system (Fig. 1) (Kreemer et al., 2010; dePolo and dePolo, 2012). Farther west, a gap in left-lateral systems exists, but they pick back up at the Rock Valley Fault which nearly connects into the Eastern California Shear Zone and Walker Lane (Fig. 2). The extent of the left-lateral system plays a role in establishing the boundary zone between the NBR and CBR.

The PSZ lies in the central part of the boundary between the NBR and CBR sub-provinces in southern Nevada (Figs. 1 and 3). Consequently, understanding the deformation style and history of the PSZ is critical to understanding the sub-province boundary, and thus, the Basin and Range province as a whole. The PSZ (a.k.a. Pahranagat fault zone, Pahranagat fault system) includes a set of three major left-lateral strike-slip faults that strike generally NE-SW. These faults, from north to south, are the Arrowhead Mine Fault, Buckhorn Fault (BF), and the Maynard Lake Fault. The PSZ deforms Paleozoic miogeoclinal strata that were previously deformed during the Sevier orogeny, Cretaceous to Oligocene non-marine sedimentary rocks, Oligocene to Miocene tuffs, and post Miocene to Quaternary alluvial and fan deposits (Tschanz and Pampeyan, 1970; Jayko, 1990). Jayko (1990) identified at least three ages of deformation within the vicinity of the PSZ, including: (1) Sevier related shortening, (2) pre-middle Oligocene extension, and (3) post late Miocene extension including strike-slip transfer faults. Jayko (1990, 2007) also identified several folds, associated with extension, within the Oligocene to Miocene tuffs, including drag folds. The PSZ has been considered tectonically active due to the presence of Quaternary fault scarps, recorded seismicity, and GPS velocity vector data (Jayko, 1990, 2007; Kreemer et al., 2010, 2012).

To enhance our understanding of the NBR-CBR boundary, including left-lateral deformation in the region but focusing on the PSZ, I undertook a detailed study including and in the vicinity of the western BF, west of U.S. highway 93 (Fig. 3). The well exposed structures in this area reveal the internal deformation, including structures and their timing, of the western PSZ. The goals of this research are: (1) to define the boundary zone between NBR-CBR, (2) understand the role paleorelief played within the PSZ, (3) map and develop a 3D geometric model of the BF and its related structures, (4) link the Paleozoic rocks within the PSZ to the

Sevier Orogenic Belt/Gass Peak thrust hangingwall or footwall rocks, and (5) consider the modern seismicity and transfer zone relationship. Fault sets and networks are used to define the specific relationships between and among faults within the PSZ, and give us insight into the transfer zone concept.

In many cases, strike-slip faults like those in the PSZ are transfer faults or zones, which are common in extensional settings, but for which a variety of definitions exist (e.g., Morley et al., 1990; Gawthorpe and Hurst, 1993; Schlische and Withjack, 2009). Faulds and Varga (1998) defined transfer zones as discrete zones of strike-slip and oblique-slip faults that strike parallel to the extension direction and assist in transferring strain between two or more extended domains. Peacock (2002) defined a transfer zone as an area between two normal faults that overstep one another, which can be further divided into conjugate and synthetic types. Kreemer et al. (2010) and Peacock (2002) give us two vastly different scales of transfer zones that are related to the resolution of their studies. Kreemer et al. (2010) delineated a transfer zone across hundreds of kilometers, whereas Peacock (2002) referred to the individual interactions between faults. Kreemer et al. (2010) connected several systems of faults within which Peacock's (2002) and Faulds and Varga's (1998) types of transfer takes place.

In addition to the sinistral faults, the PSZ contains numerous normal and oblique slip faults; to best describe the structural characteristics of the PSZ this paper will use two distinct terms, fault set and fault network. Fault sets are defined as groups of faults with similar strikes and age ranges. Fault networks are a system of multiple faults or fault sets that collectively have different strike directions but have the same age range (e.g., Peacock et al., 2016). Thus, these faults all formed and were active at the same time, despite their different strike directions, and

may accommodate triaxial (3D) strain. Figure 4 displays these sets and networks in the study area. Using only fault sets to characterize a structural region is possible when the area is undergoing no change in shape of a volume, as in classic pure or simple shear. However, fault networks should be used when describing areas undergoing triaxial strain, which has a change in three dimensions.

GEOLOGIC SETTING

Understanding the PSZ and its relationship to the surrounding geology requires regional geologic information. This includes information on the Sevier orogenic belt, Paleogene unconformity, Basin and Range province, Caliente-Enterprise Zone, and the Rock Valley fault.

The Sevier orogenic belt contains Proterozoic, Paleozoic and Mesozoic rocks that were deformed in a shortening event derived from the subduction of the Farallon Plate under the North American Plate. The Sevier orogenic belt is a segment of the larger Cordilleran retroarc fold-and-thrust belt, dating from the Late Jurassic to Eocene, which was responsible for about 220 km of crustal shortening and 16 km of crustal thickening (Dickinson, 2004; DeCelles & Coogan, 2006). The Gass Peak thrust and its associated hanging wall anticline are parts of the Sevier fold-and-thrust belt that are cut by the PSZ (Taylor et al., 2000; DeCelles and Coogan, 2006). The portion of the Gass Peak thrust in the Sheep Range, just south of the PSZ, places Neoproterozoic and younger rocks over units as young as Pennsylvanian (Fig. 2; Jayko, 2007). The Gass Peak thrust loses displacement northward and nearest the BF appears to place Cambrian rocks over Pennsylvanian rocks (Taylor et al., 2000; Jayko, 2007).

The contact between the Paleozoic rocks, which were deformed in the Mesozoic, and the Cenozoic tuffs is known as the Paleogene unconformity. Different regions of the remnant Sevier hinterland that had high topographic relief prior to Paleogene deposition (Long, 2012). Some of the topographic highs are from Oligocene or Eocene normal faulting; however, uplifted interior parts of the Sevier thrust belt have been around and eroding since before the Oligocene (Long, 2012). Thus, ~Cretaceous topographic highs composed of Paleozoic rocks

were present prior to the deposition of the Oligocene-Miocene ash-flow tuffs and influenced how these quasi-fluvial tuffs were deposited.

The PSZ lies within the Cenozoic Basin and Range province, which can be can be divided into four distinct sub-provinces including the Southern Basin and Range, CBR, NBR, and Northwestern Basin and Range (Fig. 1). Extension in the Southern Basin and Range sub-province began ~25 Ma (Sonder & Jones, 1999). Extension in the NBR started ~55 to 45 Ma with the earliest extension starting in the north (Sonder & Jones, 1999). Miocene extension in the Great Basin began around 17.5 Ma (Dickinson, 2006). Shortly after (17 to 14 Ma) that, magmatism started in the backarc of the Pacific Northwest which coincided with further deformation in the entire Basin and Range, including the Great Basin (Dickinson, 2006). Thus, by the Oligocene to early Miocene both the NBR and Southern Basin and Range sub-provinces were extending or had extended. This left the unextended CBR at a relatively high stress load. Eventually, the high stress load would lead to rock failure and, thus, the beginning of extension in the CBR at 18 to 14 Ma (Sonder & Jones, 1999; Bidgoli et al., 2015). Specific timings and magnitudes of CBR structures include the Saddle Island Detachment accommodating 20 km of westward migration of upper-plate rocks post 13.5 Ma (Duebendorfer et al., 1990), the Mormon Peak Detachment accommodating a maximum of 10.9 to 19.5 km of extension post 14-12 Ma (Walker et al., 2007; Bidgoli et al., 2015), the Tule Springs Detachment potentially accommodating as much as 5-7 km of exhumation on the Tule Springs Hills post 14 Ma (Bidgoli et al., 2015), and the Castle Cliffs Detachment which initiated up to 5 m.y. before the Tule Springs or Mormon Peak Detachments with 7-8 km of exhumation taking place on the Beaver Dam Mountains post 18 Ma (Bidgoli et al., 2015). The differences in timing of the onset of extension between the NBR and CBR, and the

occurrence of multiple episodes of extension in the NBR allow the development of multiple generations of extension with the potential for superimposed structures (Taylor & Switzer, 2001). The crust under the Northwestern Basin and Range sub-province, ~38 km thick in the Late Cretaceous, was not as thick as the crust under the NBR, which was at least 45 km thick and, thus, did not undergo as much post-Late Cretaceous extension (Colgan et al., 2006).

The Caliente-Enterprise Zone is located northeast of the PSZ and is characterized by multiple episodes of extension beginning before 30 Ma (Fig. 2). The Caliente-Enterprise Zone can be divided into three parts: (1) the eastern part, which is associated with the Colorado Plateau margin; (2) the central part, which is within the Caliente Caldera Complex; and (3) the western part, which is associated with PSZ faults (Axen, 1998). The Caliente-Enterprise Zone is thought to have disrupted the extension from nearby detachment faults and instead was internally extended (Axen, 1998). This internal extension resulted in the formation of multiple strike-slip faults and fault blocks with counterclockwise vertical-axis rotation (Axen, 1998; Hudson et al., 1998). Paleomagnetic data document that the Caliente-Enterprise Zone is a broad sinistral transfer zone with vertical-axis rotation of blocks (Hudson et al., 1998). Importantly, the paleomagnetic data show that the some of the mildly counterclockwise rotated blocks of the Caliente-Enterprise Zone extend into the PSZ, thereby linking the Caliente-Enterprise Zone and PSZ directly into one another (Hudson et al., 1998).

The Rock Valley Fault Zone is a left-lateral fault zone located to the west of the PSZ and between these two zones is an area of predominantly normal faulting (Fig. 2). The Rock Valley Fault Zone is a 20-40 km long, several kilometers wide, east- to northeast-striking left-lateral fault zone (O'Leary, 2000). Within the Rock Valley Fault Zone are three >18 km long left-lateral faults that are roughly oriented N70° E, until becoming more southward in

orientation near the Specter Range. The zone of normal faulting between the Rock Valley Fault Zone and PSZ is 90-100 km wide.

METHODOLOGY

An area of approximately 36 km^2 around the western part of the BF was mapped at a 1:12,000 scale to obtain spatial, geometric and kinematic data (Plate 1). Field data were collected using standard mapping methods on a U.S. Geological Survey topographic base map aided by satellite, 1997 orthophotos and 2010 NAIP imagery, and limited GPS location data. Bedding, compaction foliation in tuffs, fault surfaces, and other linear and planar features were measured with a Brunton compass. Samples of Kane Wash Tuff subunit 3 were collected and brought to laboratories to both make and analyze a thin section, and acquire an ^{40}Ar/^{39}Ar date.

Laboratory analyses were conducted on selected samples to further support the field identification of tuffs used to constrain the timing of deformation. Point counting was done to the same sample that was dated to make sure it correlated to the correct unit. A thin section of Kane Wash Tuff subunit 3 was point counted using a petrographic microscope with a point counting stage that created a grid-like counting system (Appendix B). A total of 1,200 points were counted. This number of points was counted to acquire a reliability greater than 90% (Van der Plas and Tobi, 1965).

^{40}Ar/^{39}Ar dating was conducted to better constrain the timing of deformation along the BF by dating the stratigraphically highest tuff, the Kane Wash Tuff subunit 3. Kane Wash Tuff subunit 3 samples were crushed in laboratories at UNLV and sorted by grain sizes via sieves. Sieve sizes used were 60 and 120. The largest sanidine crystals without matrix attached were then handpicked with the aid of a microscope and fine point brush. Crystal grains were then put into a sonic bath to remove any remaining matrix material clinging to the crystal. The crystals were then sent off for irradiation, done at the United States Geologic Survey TRIGRA

Reactor in Denver, Colorado, and then analyzed in the NIGL laboratory at UNLV. $^{40}Ar/^{39}Ar$

analysis was performed using a multi-crystal laser heating system after unreliable results were

acquired by single-crystal analysis (Appendix 3). I ran 5 of the multi-crystal analyses with the

direct help of experienced laboratory technician, Kathleen Zanetti. This process included

fusing together the irradiated samples of sanidine with CaF^2 and K- glass fragments using a

20 W CO^2 laser. A stage positioned the samples correctly under the laser and a video camera

was used to display the stage to myself and the lab technician (Appendix 3).

Data collected from the field and three-point problem calculations were used to construct and

plot stereographs and cross sections of fold, fault and bedding data. Stereographs were plotted

using Rick Allmendinger's *Stereonet 9* program (Allmendinger, 2015).

STRATIGRAPHY

Stratigraphy around the western BF, within the mapped region (Fig. 5), includes Paleozoic carbonates and quartzites, Cretaceous or Tertiary (Paleogene) conglomerate, Oligocene-Miocene tuffs, and Quaternary alluvium (Figs. 6 and 7). These units have been previously identified and mapped at a 1:100,000 scale by Jayko (2007). However, attached unit descriptions (Plate 1) refine these units to more localized descriptions with subdivision into individual regional formations of the tuffs following Best et al. (1993, 2013a, b).

The Paleozoic rocks consist of carbonates, including both limestone and dolostone, and sandstones, which are silica-cemented sandstone (Fig. 7). From oldest to youngest, the exposed units are the Ordovician Eureka Quartzite and Ely Springs Dolomite, followed by the Silurian Laketown Dolomite and Devonian Sevy Dolomite (Reso, 1963; Tschanz and Pampeyan, 1970). These units were faulted into place during the Sevier orogeny (Burchfiel, 1965; Ebanks, 1965; Guth, 1980; Taylor et al., 2000; DeCelles and Coogan, 2006). These rocks were exposed by erosion and/or Cenozoic normal faulting (Long, 2012). The Paleozoic rocks are overlain in buttress unconformity by all of the younger units in the area. Paleozoic units both older and younger than the exposed section (Plate 1) are documented in the region (Fig. 2).

A Cretaceous or Tertiary (Paleogene) conglomerate locally lies between the Paleozoic units and the Oligocene ash-flow tuffs (Fig. 7). All of the clasts in this unit are composed of carbonate or quartzite from various Paleozoic units. Near the BF the conglomerate is only about a meter thick in exposures, but the base is not exposed.

Tertiary units include ash-flow tuff, ash-fall tuff, reworked tuff, and vesicular basalt. Tertiary tuffs range from Monotony to Kane Wash tuffs (Plate 1, Fig. 6). These tuffs were erupted from three different source areas: (1) the Central Nevada Caldera Complex, (2) the Caliente Caldera Complex, and (3) the Kane Springs Wash Caldera (Fig. 2) (Best et al., 2013a, b). Ages below are from Best et al. (2013a, b). The Central Nevada Caldera Complex produced the 27.57 Ma Monotony Tuff, multiple cooling units of the 25.99-26.98 Ma Shingle Pass Formation and the 22.93 Ma Pahranagat Formation (Best et al., 2013a). The Caliente Caldera complex produced the 23.04-24.15 Ma Condor Canyon Formation, 24.03 Ma Leach Canyon Tuff, 22.56 Ma Harmony Hills Tuff, and 18.51 Ma Hiko Tuff (Best et al., 2013b). The Kane Springs Wash Caldera produced the Kane Wash tuffs. An $^{40}Ar/^{39}Ar$ age was obtained from analysis of the uppermost welded member of the Kane Wash Tuff (Tk3) and yielded a date of 15.3 +/- 0.09 Ma. Basalts are located on top of the Tertiary tuffs (Jayko, 2007) and primarily occur as float exposed in a single hill in the northwest section of the map (Plate 1, Fig. 5).

The Quaternary stratigraphy is divided into two major units: (1) Quaternary alluvium and (2) Quaternary older alluvium. Quaternary alluvium is the young detritus in active/recently active washes and fans. Quaternary older alluvium includes all detritus that was not active recently including, but not limited to, older, now abandoned, drainages and alluvial fan deposits that display ridge and ravine topography. Quaternary older alluvium has a degree of compaction and possibly slight calcite cementation that lithifies the material.

STRUCTURAL DATA

The BF lies between the Arrowhead Mine Fault and Maynard Lake Fault, and thus, is flanked by structures that accommodate differences in motion between each of these left-lateral strike-slip faults and the BF. Therefore, structures are divided into those northwest and southeast of the BF. Previous mapping and structural analyses (Tschanz and Pampeyan, 1970; Jayko, 2007) lack the map resolution necessary to adequately analyze and interpret the structural complexity of the BF and associated structures. Therefore, my new 1:12,000 scale map is used here (Plate 1). The mapped area contains strike-slip and normal faults, and folds (Fig. 4).

The Buckhorn Fault

The BF is a left-lateral strike-slip fault with a 030-040º strike through much of the map area, but bends to strike 070-080° in the southwest (Plate 1, Fig. 4). The BF splays along strike forming many small bends with several fault blocks or lenses trapped between the strands. These fault blocks contain normal faults exposed in Tertiary tuffs. The BF is almost entirely buried under active Quaternary alluvium with a single exposure in the NE portion of the map (Plate 1). The exposed strand places Kane Wash Tuff against Hiko Tuff and has an attitude of 035°, 76° SE. After 15.3 Ma, the BF had at least 6 kilometers of left-lateral strike-slip offset based on offset of the base of the Kane Wash Tuff and less than 250 meters of down to the north dip-slip offset based on elevation differences from the cross-sections between the contacts of Tk1 and Tk2, and Hiko and Harmony Hills tuffs directly north and south of the BF. The BF decreases in strike-slip offset to the west. A few meters west of a series of splay faults in the west, the offset is ~ 5-20 m (Plate 1) (Price et al., 2017). On the western end, the BF abuts into, or is cut by, a north-south striking normal fault (Plate 1, Fig. 4).

13

Northwest of the Buckhorn Fault

The Buckhorn Syncline (BS), named here, is a few kilometers across and located just north of the BF. In exposures, units from the Monotony Tuff to the Kane Wash Tuff are folded (Plate 1, Figs. 4, 5 and 8). The fold is best exposed in the Hiko Tuff (Plate 1, Fig. 5). The BS plunges and trends 27°, 032° and is subparallel to the BF (Figs. 4 and. 9). The BS limbs generally dip around 20-35º making a gentle to open fold. Overall the BS axial surface is upright, dipping 87°, with a gentle interlimb angle of 153º. The southeastern limb of the syncline is cut by the BF.

The Buckhorn Anticline (BA), named here, lies east-southeast of the syncline axial surface, but the two folds are not parallel. The BA refolds the southeastern limb of the BS. The amplitude of the BA decreases towards the axial surface of the BS as is suggested by the BS's axial surface not being deflected. The anticline is gentle with a steeply dipping, upright axial surface and has a plunge and trend of 15º, 010° (Figs. 4 and 9). This fold was only identified in the Hiko Tuff.

The region northwest of the BF contains at least three sets or networks of normal or normal-oblique slip faults including (1) an E-W striking fault set in the NW section of the map (Fault set NA); (2) NNE-SSW striking faults that occur near the west end of the BF (Fault set NB), one of which cuts an E-W striking fault; and (3) faults with a variety of strikes that occur within the fold (fault set NC) (Fig. 4, Plate 1). These structures all were identified by offsets of Tertiary tuffs (Plate 1).

The E-W striking faults with apparent normal offset dip to the south. This fault set (NA) includes four faults in the NW corner of the map which are exposed cutting the Monotony

through Hiko tuffs and are truncated by the Kane Wash Tuff, thus bracketing deformation time to between 18.41 and 15.3 Ma. This fault set varies from 20 m to >100 m of stratigraphic offset and has a slight apparent left-lateral slip.

An E-W fault, fault N1, is exposed in Tertiary tuffs and has a small stratigraphic offset putting Bauers Member next to Pahranagat Formation (less than 30 m) and lies in a fault-bounded block near the west end of the BF (Fig. 4). This fault is characterized by a weak friable zone between these two stratigraphic units of steeply dipping (62-76º) tuffs. This fault is primarily normal and lacks any significant apparent lateral offset. This fault terminates into fault N2 that directly connects to the BF.

Fault network NC consists of two faults exposed near the fold core and two faults cutting the western limb which have a variety of strikes and cut tuffs from the Bauers Member to the Kane Wash Tuff (Fig. 4). The faults in the core are primarily normal and all cut the BS axial surface. The two faults along the northwest limb of the fold are near the fold axial surface but do not cut it and are exposed within the Bauers, Pahranagat, and Harmony Hills tuffs. These faults vary from E-W to N-S in strike and are grouped based on their relationship to the fold and their uncertain relationship to other structures.

Southeast of the Buckhorn Fault

The area southeast of the BF contains the Paleogene unconformity and normal to oblique faults exposed within Tertiary tuffs and Paleozoic carbonates. These faults are divided into a fault set and a network. Fault set SA consists of two large normal faults, which abut into the BF. Fault network SB comprises small faults that run between the larger normal faults of SA.

Two faults of SB strike ~E-W, others strike WNW and all cut the Paleozoic strata in exposures. Fault set SA and network SB form fault network FNS.

The two large normal faults of set SA strike NNW-SSE to NNE-SSW and have a minimum map length of 3-5.5 km. These large faults are entirely buried under Quaternary deposits but are known to exist because of retro-deformations of cross sections using nearby exposed tuffs (Plate 2). This fault set contains the largest fault in the map area exclusive of the BF (Plate 1, Fig. 4). These faults have relatively large stratigraphic offsets, up to 1 km, and abut into the BF.

Eight smaller faults compose fault sub-network SB and are kinematically associated with fault network SA. Faults of SB generally strike ENE-WSW, WNW-ESE and NW-SE. In exposures, the NW-striking faults cut units from Monotony to Harmony Hills tuffs (Figs. 4 and 5; Plate 1). These faults are generally apparent normal with one having some apparent right-lateral offset. The ~E-W striking faults cut the Paleozoic units and put Silurian Laketown Dolomite next to Devonian Sevy Dolomite. The northern fault terminates into a strand of the BF to the west and terminates into the large N-S buried fault of SA to the east. Field identification of this fault can be subtle, but cross sections and orthoimagery support the presence and location of this structure.

Fault S1 is cut by the BF and cuts units up to Harmony Hills but is buried under the Hiko and Kane Wash tuffs (Figs. 4 and 5; Plate 1). Thus, the fault is bracketed to a deformation time between 22.56 to 18.51 Ma. The fault is exposed for 70 m along strike. This is the only fault identified in the field area that has this timing.

Fault network SC (mapped by R. A. McIntyre, W. J. Taylor and myself) consists of several splay faults that generally strike NE-SW near the BF through N-S and curve to a more NW-SE strike in the south (Fig. 4). These faults are normal faults with down-to-the-east offset. The individual faults within this network vary between the ~6.4 km long splay faults and the < 0.5 km smaller faults that run between these splays. The total offset of this network helps to form a basin between SC and the farthest west normal fault of SA, currently filled with Tertiary and Quaternary alluvium and fan deposits.

Paleogene Unconformity

The Paleogene unconformity is exposed in the field area as a block of Paleozoic rocks with Miocene-Oligocene tuffs and a Tertiary (Oligocene?)-Cretaceous conglomerate abutting into it (Plate 1 and 2; Fig. 10). The Paleogene unconformity has a minimum of 240 meters of relief directly north of the BF, from the fence diagram, but has a minimum of 600-700 meters south, along the exposed Paleozoic block (Plate 2; Fig. 10). The angle across the unconformity varies from 45-49°. The exposed Paleozoic hill has no tuffs deposited on top of it, unlike some of the Paleozoic mountains seen off to the East along highway 93 (location X on Fig. 3), which indicates that the ash-flow tuffs did not fill all the way to the top of the hills along the unconformity.

DISCUSSION

PAHRANAGAT SHEAR ZONE GEOLOGY

Northern to Central Basin and Range boundary zone

The PSZ defines the central part of the boundary zone between the NBR and CBR

subprovinces and the Caliente-Enterprise Zone defines the boundary to the east. This left-

lateral zone is extrapolated to the west, in this study, (Fig. 1) by using Bouguer gravity,

magnetic, basin elevation data, and previous work on the Rock Valley Fault Zone (O'Leary,

2000). Map data show that structures internal to the PSZ accommodate motion and

differences in slip along the Arrowhead Mine and Maynard Lake Faults because faults and

folds near the western BF continue to the northwest and southeast but do not cut the

Arrowhead Mine or Maynard Lake Faults (c.f., Price et al., 2017). Thus, the faults and folds

within the PSZ do not necessarily kinematically link to either the NBR or CBR structures

(Fig. 2). The largest of these internal accommodation structures is the BF. This internal, to the

PSZ, deformation delineates the boundary between the NBR and CBR as a zone rather than a

single structure or finite line. Thus, the boundary zone uses the outer extents of these left-

lateral systems as the boundaries, leaving the internal deformation of these zones as part of

the newly defined zone.

The western limit of the PSZ is structurally bounded by large north-south striking normal

faults and geographically marked by the Desert Hills (Figs. 3 and 4). A series of these north-

south striking normal faults extend throughout the region between the PSZ and the Rock

Valley Fault Zone. Thus, the zone between the NBR and CBR subprovinces is weakly

constrained and loosely defined by gravity anomalies and basin elevations through that region.

Cretaceous to Oligocene(?) Paleohill

Directly southeast of each major PSZ fault, the Arrowhead Mine Fault, BF and Maynard Lake Fault, are exposed hills or mountains made of Paleozoic rocks (Fig. 3) (Jayko, 2007; Price et al., 2017). The buttress unconformity between Paleozoic rocks in these hills and the Oligocene to Miocene tuffs along with the deposition of the Tertiary to Cretaceous conglomerate suggests that these exposed hills of Paleozoic strata must have been relatively high before and during the deposition of the tuffs. Normal faulting contributed to exposing this relationship by relatively down dropping Tertiary tuffs along faults of SA on either side of a horst that exposes Paleozoic rocks (Fig. 11). South of the BF hundreds of meters of Leach Canyon is exposed to the west of the paleohill and only about 12 meters to the east (Plate 1). This result could be from the thinning of these tuffs, related to the quasi-fluvial flow patterns of ash-flow tuffs around the hill, the locations of the source calderas relative to the study area and Paleozoic hill locations. Similarly, north of the BF, differences occur in the ash-flow tuff stratigraphic section, with exposure of the Leach Canyon and Bauers Tuffs being prominent in the southwest, the lack of the Pahranagat Tuff in some areas, and unit thickness changes within the Harmony Hills Tuff. (Plates 1 and 2; Fig. 10). An additional, buried, paleohill and faulting is a simple and the most supported solution for the differences in tuffs north of the BF (Fig. 10, Plate 2). This additional paleohill could account for the lack of Leach Canyon and Bauers tuffs, which were sourced from the northwest, being exposed on the east side of the map, north of the BF.

LOCAL GEOLOGY

Buckhorn Fault

The changes in amount of offset, bends, splays, and fault blocks of the BF indicate a non-planar fault geometry that is likely controlled by fault-linkage and/or pre-existing structures (Plate 1; Fig. 4). The best evidence for this interpretation is the offset (>6 km) measured just east of the bend from a NE- to ENE-strike in the BF, compared to the <20 meters along the southwest part of the BF. These differences could be explained by two faults that had a smaller offset and a larger offset before they linked into one continuous strand. Another potential solution is the SW propagation of the BF accounting for the loss of slip westward along the BF, but not necessarily for the bend or magnitude of slip loss.

West-end of the Buckhorn Fault

The BF terminates within the map area, abutting into fault set NF1. Prior to abutting into fault set NF1, the BF propagated to the west, as suggested by the decrease in offset westward. Offset along the main strand of the BF decreases from 6- 6.5 km in the eastern part of the study area, when considering the offset of the contact between the Hiko and Kane Wash tuffs, to just a few meters (5-20), based on offset of the contact between the Tertiary Leach Canyon and Bauers tuffs, about 6-8 km to the SW (Location Z on Plate 1 and Fig. 5). Map data show that the offset decreases significantly just west of the splays near the center of the map, which are in fault network SC (Fig. 4). Fault network SC is a strong candidate for distributing strain away from the BF as it propagated SW. The BF is exposed up to a few meters away from a several kilometer-long normal fault, part of fault network NF1, but does not extend west of this network. This is likely the result of the BF being soft- or hard-linked to the NF1 fault in

20

the subsurface (Price et al., 2017) (Fig. 4). If so, this suggests that the BF transfers a small amount of strain onto fault network NF1.

Buckhorn Folds

Folds can form in association with strike-slip faults in extensional settings (Harding, 1976; Sylvester, 1988; Jayko, 1990; Becker, 1995; Grasemann et al., 2005). The parallelism between the BF and BS suggests that the two are related. The BF and BS geometries permit multiple interpretations of how the BS could have formed. These include, but are not necessarily limited to: (1) a drag or fault propagation fold formed from changes in slip along the BF, (2) a fold formed by a wedge between two faults that decreases in volume along strike, or (3) a separate deformation event older than the BF (Figs. 4 and 11). Option 2 can be ruled out because the BS is in an area of widening between the Arrowhead Mine Fault and BF (Price et al., 2017). Option 3 can be ruled out because the fold deforms the Kane Wash Tuff, the youngest ash-flow tuff, and thus, formed after 15.3 Ma when the BF was active. The orientation of the BS, with a trend of 032°, the scale and proximity of the BS to the BF (Fig. 4), and changes in offset along strike of the BF along with the <10° angle between the axial surface and the nearest segment of the BF would suggest that the fold formed as a result of option 1, drag or fault propagation.

The BA is superimposed on a limb of the BS and is isolated between the BF and the axial surface of the BS (Figs. 4 and 5). The axial surface of the BA is at a 20-30° angle to the BS's axial surface, not parallel or subparallel. The superposition of the BA suggests that it formed after the BS and the difference in orientation suggests that it potentially formed from a different or changing localized stress field.

21

The nonparallel fold axes, along with the limited length of the BA, leads to the possibility of a multistep formation. Unfortunately, the data are not definitive enough to completely limit the conclusion down to a single outcome. Thus, multiple possibilities must be considered including four reasonable options all having the BS formed from drag along or propagation of the BF. (1) The BA was superimposed on the BS due to local stress field changes related to a bend in the BF. The bend in the BF from ~N30°E to ~N70° E would create a proximal area of shortening (Fig. 4). However, the orientation of the bend combined with left-slip on the BF would create a primary shortening direction of NE-SW with folds oriented NW-SE. This expected trend is opposite of the BA's current axial surface trend. (2) The BA formed later as a result of a wedge forming between the BF and fault N2 (Fig. 4). In this case, the normal fault/fault block would have to act as a barrier, and thus, the shortening direction would be E-W. The initial strike of the BA's axial surface would then be nearly N-S. Continued motion along the BF would drag this fold into a NW-SE trend, opposite of its current position. (3) Multiple circumstances played a role in the formation of the BA. This scenario allows for multiple conditions to play a role in the formation of the BA and might explain why the angular relationship between the BA and BF cannot be explained from previous foundational studies like Sylvester (1988) and such as listed in options 1 and 2. These multiple conditions: (a) continued motion along the BF, (b) motion along fault N2, (c) transpression from the bend in the BF and (d) the influence of the pre-existing weaknesses in the rheology. (4) None of the drag, wedge or bend mechanisms are responsible for the formation of the BA (Fig. 4). This scenario is a possibility but is not as probable as option 3, because nearby structures namely the bend in the BF and fault N2, logically have some effect on the nearby local stresses.

Option 3 is the most likely scenario of the options listed above, as it accounts for the scale, exposure, trend, and temporal relationships previously discussed.

East-West striking faults

Fault set NA (colored in light blue on Fig. 4) strikes at an angle approximately perpendicular to the major normal faults within the mapped area and are post-18.51 to pre-15.3 in age (Figs. 5, 10; Plate 1). Faults of set NA have apparent normal slip with a high potential for a notable amount of strike-slip motion because of the amount of pure dip-slip required to put the Hiko Tuff next to Shingle Pass Tuff (450-480 meters) in comparison to the exposed lengths of the faults (300-500 meters) (Plate 1). The strike-slip motion would dramatically decrease the amount of stratigraphic offset needed to account for map data (Plate 1) from >450 m to <100 m of dip slip. In the case of pure strike-slip motion, one fault would have to be left-lateral and the other would need to be right-lateral, each with minimum of 2 km of slip. Oblique-slip would allow these faults to accommodate both or either of two different local stress fields presented in the local area. First, the angle of ~70-85° between this fault set and the BF fits with the expected angle of strike with antithetic R' shears related to motion along the BF (Sylvester, 1988) (Fig. 4). Second, the local extensional stresses applied from the opening of the gap between the AMF and BF can be partially accommodated by the normal-slip (Fig. 3) (Price et al., 2017). This gap is a function of the 030-040° strike of the BF relative to the average 042° strike of the Arrowhead Mine Fault in the west side of the PSZ (Fig. 3).

Associated normal faults

The normal faults, within proximity of the BF, can be placed into three categories: (1) faults that strike at a high angle to the BF, (2) faults that transfer strain between two faults, and (3)

faults that distribute strain. The high-angle faults are fault sets NB and SA and suggest that the BF is a transfer fault. The faults within fault set SB and N1 transfer strain between two faults; SB transfers strain between two SA faults and N1 transfers strain from two NB fault strands. Fault set SC consists of faults distributing strain at a paleotip away from the BF (Fig. 4). These geometric relations between normal faults and strike-slip faults were recognized and characterized by Sylvester (1988) and Peacock et al. (2016).

Fault network FNS consists of fault sets SA and SB. The normal faults of fault network FNS, have cross-cutting relationships in which faults within fault set SB have strikes between NW-SE to E-W and abut into fault set SA and the BF. Faults within SA strike north to south and abut into the BF (Fig. 4). This relationship of faults abutting into, but not cutting through, each other suggests that motion along these faults are not temporally distinct from one another. This synchroneity lead to a volume growth or change in shape in the area south of the BF. Consequently, triaxial strain occurred. The rock volume would have thinned vertically due to the normal faults, lengthened horizontally in both a N-S and E-W directions and changed shape, especially along the BF and NW-striking faults near it (Fig. 4).

Timing of deformation

The western BF region, west of U.S. highway 93, exposes at least four different ages of deformation: (1) tilting of the Paleozoic rocks to a dip of 50-60° prior to emplacement of the 27.57 Ma Monotony Tuff, (2) an episode of early-Miocene deformation between 22.56 and 18.51 Ma, (3) mid-Miocene deformation between 18.51 Ma and 15.3 Ma, and (4) deformation after deposition of the Kane Wash Tuff (15.3 Ma). The tilting of the Paleozoic rocks most likely occurred during the Sevier orogeny because of the proximity to other Sevier belt structures and the angularity of the Paleogene unconformity. This deformation uplifted the

Paleozoic rocks which were subsequently eroded forming paleohills. The early-Miocene

deformation is represented by a single NW-SE striking fault, fault S1, putting Harmony Hills

Tuff next to Shingle Pass Formation and Bauers Member and is overlain by the Hiko Tuff

(Plate 1, Figs. 4 and 5). This timing of this fault coincides with deformation in the NBR, but

pre-dates major extension in the CBR. The mid-Miocene deformation is represented by four

WNW-ESE-striking faults, fault set NA, which are all overlain by the 15.3 Ma Kane Wash

Tuff. Lastly, the post 15.3 Ma deformation includes the BF, BS, BA, large normal faults and

many other structures all of which can be organized in relation to each other via cross-cutting

and abutting relationships. The BF formed as a result of two possible options: (1) a new fault

or (2) an older reactivated fault that breaks through the Oligocene-Miocene tuffs. The older

structure, prior to reactivation, does not need to be right-lateral (Jayko, 1990) if the Paleozoic

section is a part of the footwall of the Gass Peak Thrust (discussed below). The BS formed in

the fourth deformation either at the same time as or just before the BF. Several of the fault

sets and networks with a variety of orientations formed at this time.

REGIONAL GEOLOGY

The Gass Peak Thrust

The exposed Paleozoic strata, from Devonian to Ordovician in age, are part of either the

footwall or hangingwall of the Gass Peak Thrust (Fig. 2; Plate 1). The Paleozoic strata within

the field area are relatively undeformed internally and currently have a 20-40° W dip.

However, before Oligocene-Miocene extension the strata dipped at a much steeper angle,

perhaps greater than 60°. This higher dip comes from removing the current 10° to 35°

eastward dips of the unconformably overlying Oligocene to Miocene tuffs. The internal

deformation of nearby exposed footwall sections show moderately dipping to overturned beds

25

and folding (Page et al., 1990, Swadley et al., 1994; Jayko, 2007). Presently hanging wall sections seem relatively undeformed or are part of a range-scale anticline and generally dip east. Strata that are clearly in the footwall of the Gass Peak thrust just south of the Maynard Lake Fault and east of U.S. highway 93 in the Delamar Mountains, similar to the study area, are moderately W-dipping Paleozoic rocks that are unconformably overlain by gently E-dipping Tertiary ash-flow tuffs (Fig. 3; c.f., Scott et al., 1990). These nearby examples of foot- and hanging-wall strata each share a bit in common with the exposed section of Paleozoic rocks within the field area. Thus, the shared W-dipping direction and less slip required to retrodeform the exposed Paleozoic strata in the field area to footwall outcrops better supports the conclusion that these Paleozoic rocks are part of the footwall of the Gass Peak Thrust.

Transfer Zone

The termination of normal faults in many cases is marked by an accommodation or transfer zone (Faulds and Varga, 1998). The PSZ has a series of normal faults to the north and an area of limited extension to the south in the vicinity of the Sheep Range (Figs. 2, 3; Jayko, 2007). The normal faults to the north strike northerly which fits with the least principal stress direction, WNW-ESE to E-W, documented after 10 Ma by Zoback et al. (1981), and abut into at least one left-lateral fault of the PSZ. The relatively large N-striking normal faults, such as the faults of NF1 cut across or are abutted by the BF, as shown here, and the AMF (Price et al., 2017; Evans, in progress). In contrast, many of these faults abut into the MLF (Muhammad, 2016; Fig. 2) (Figs. 2 and 4). Faults of NF1 and other normal faults on the outer sides of the PSZ potentially transfer strain onto one or more faults of the PSZ or vice versa. GPS velocity data support that the PSZ is currently transferring strain between the

Eastern California Shear Zone and the Wasatch Fault Zone (Kreemer et al., 2010; dePolo and dePolo, 2012). Kreemer et al. (2010) defines the PSZ as part of the Southern Nevada Seismic Belt (Fig. 12). The Southern Nevada Seismic Belt is composed of seismic clusters, including seismicity within the PSZ (Fig. 12). Therefore, strain is transferred through areas both in the scale described by my work in the PSZ and in the regional scale described by Kreemer et al. (2010) and dePolo and dePolo (2012) (Figs. 4 and 12.).

CONCLUSIONS

The sub-province boundary between the NBR and CBR is here defined as a broad zone that includes significant left-lateral deformation such as that along the PSZ. The PSZ is a prominent NE-striking, left-lateral fault system with a distinct internal deformation that lies in the central part of the boundary zone.

Regional

1. The major left-lateral strike-slip faults of the PSZ define the central part of the boundary zone between the NBR and CBR. A steep gradient in the Bouguer gravity anomaly, from higher in the north to lower in the south, and left-lateral shear systems were used to extend the NBR-CBR boundary zone across the Basin and Range province (Fig. 1). In addition, the timing of initial extension is different north and south of the PSZ, whereas, deformation within the PSZ is distinct.

2. The west-end of the left-lateral strike-slip system that includes the Caliente-Enterprise Zone and PSZ ends east of the Desert Hills, which lie within the boundary zone. Offset along the BF decreases southwestward and the fault abuts into a normal fault within the study area.

Local

1. The Paleozoic strata, which dipped relatively steeply W prior to the Miocene, are part of the footwall of the Gass Peak thrust and are the base of the Paleogene Unconformity. The angle across the Paleogene Unconformity varies from 40-49° and it has a minimum relief of 600-700 meters south of the BF and 240 meters to the north.

2. Based on cross-cutting relationships, at least three ages of extensional deformation occurred within the PSZ: (Deformation 1) 22.2 to 18.6 Ma, (Deformation 2) 18.6 to 15.3 Ma, and (Deformation 3) post 15.3 Ma. The first two are defined by normal faults and the youngest by sets and networks of normal-, strike- and oblique-slip faults.

3. The BF accommodates strain between the Arrowhead Mine and Maynard Lake Faults that is recognizably different from deformation outside of the PSZ. Folding and up to 6-6.5 km of left-lateral slip occurred along the BF after 15.3 Ma.

4. The BF ends westward. A set of splay faults at the west-end of the BF accommodates the majority of slip decrease along the BF as it dies out westward. The west end of the BF abuts into a large N-S striking normal fault (NF1) and may transfer the remaining small amount of slip onto it.

5. Two episodes of localized shortening occurred post 15.3 Ma just north of the BF resulting in sequential formation of the BS and BA. The BS is a fault propagation or drag fold related to left-lateral slip along the BF based on subparallel orientations and timing. The BA likely results from interactions of multiple local structures including the BF, BS and N2 resulting in the axial surface trend of 010°. Interactions include fault linkage between N2 and the BF, potential linkage of individual isolated strands of the earlier less developed BF, and the formation of a bend within the BF.

6. In contrast to north of the western BF, triaxial strain is significant just south of the western BF, between the BF and the Maynard Lake Fault. Triaxial strain is the result of motion along fault network FNS which consists of faults with three different strikes; N-S, NE-SW, E-W.

7. The youngest mapped faults cut Kane Wash Tuff subunit 3 and are buried by Quaternary units. This relation suggests that there are no active faults within the study area.
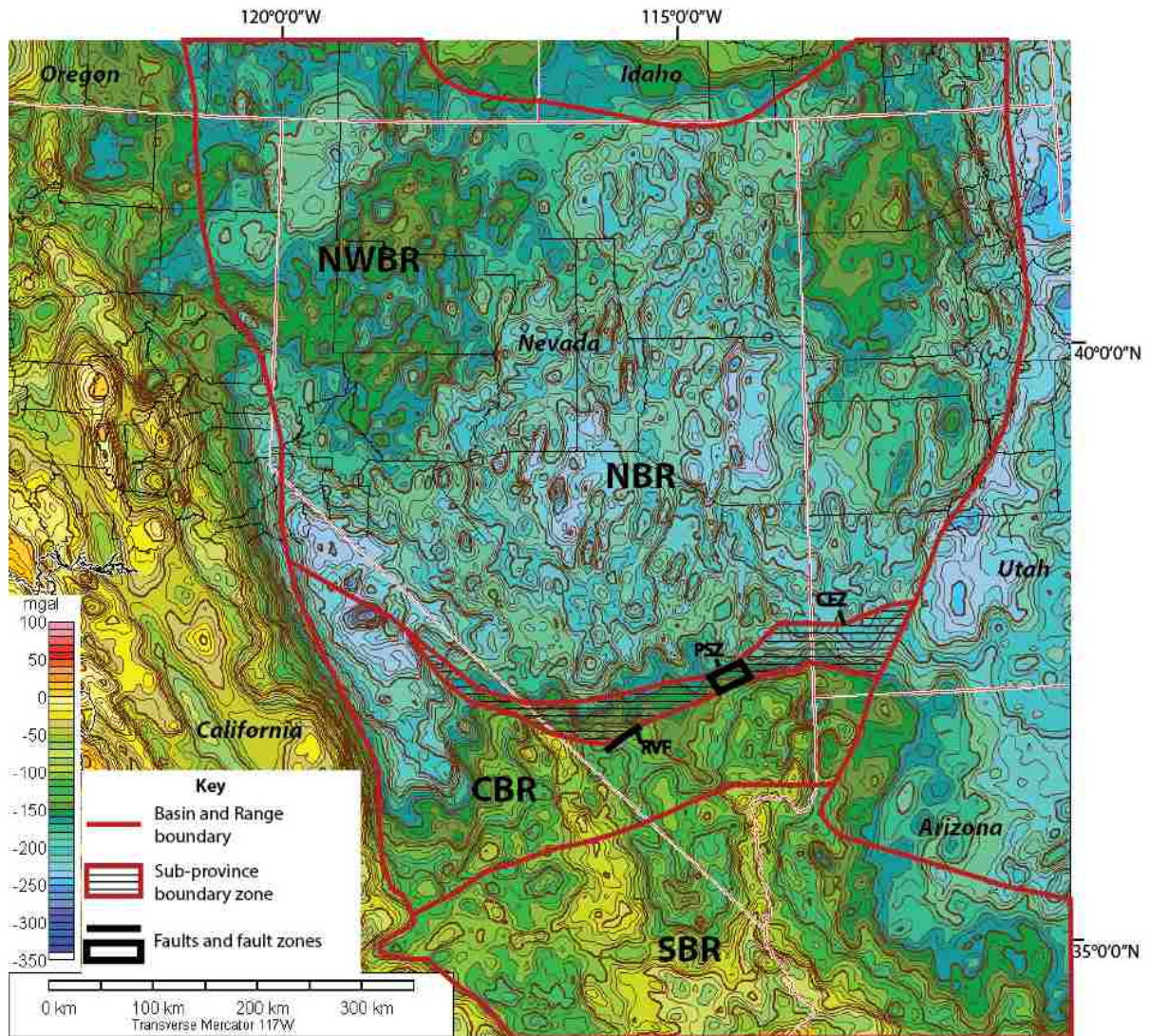
Figure 1. Regional gravity map also showing the boundary of the Basin and Range and the location of its subprovinces. NWBR – Northwestern Basin and Range, NBR – Northern Basin and Range, CBR – Central Basin and Range, and SBR – Southern Basin and Range. RVF – Rock Valley Fault, PSZ – Pahranagat shear zone, and CEZ – Caliente-Enterprise Zone. Background image is a Bouguer gravity map from Dutch (2014).
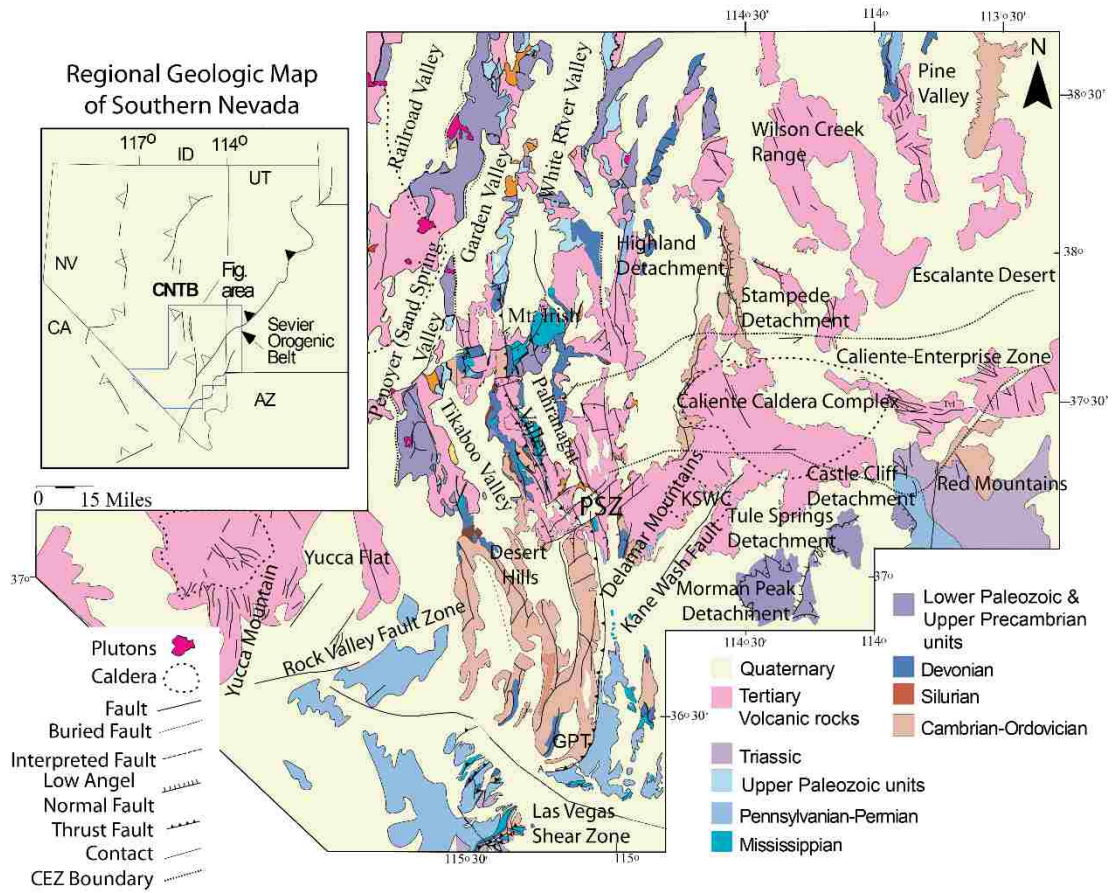
Figure 2. Regional geology map showing larger structures and simplified geologic units. PSZ – Pahranagat shear zone, KSWC – Kane Springs Wash Caldera, GPT – Gass Peak Thrust, CNTB – Central Nevada Thrust Belt. Caliente-Enterprise Zone location is based on Hudson et al. (1998).

Figure 3. A location map showing simplified geometries of the Arrowhead Mine Fault (AMF), Buckhorn Fault (BF) and Maynard Lake Fault (MLF). Study area is outlined in purple. Blue dotted line represents the Paleogene Unconformity. Yellow "X" marks the approximate location to the Paleogene Unconformity related to in thesis body text location. Tv is Tertiary volcanic rocks. The Buckhorn Syncline is in blue. Study area includes mapping done in the southwest of dotted line by Alex Peck and R. Alexis McIntyre with an additional help from Rebecca Ely, Michael Evans and Dr. Taylor.
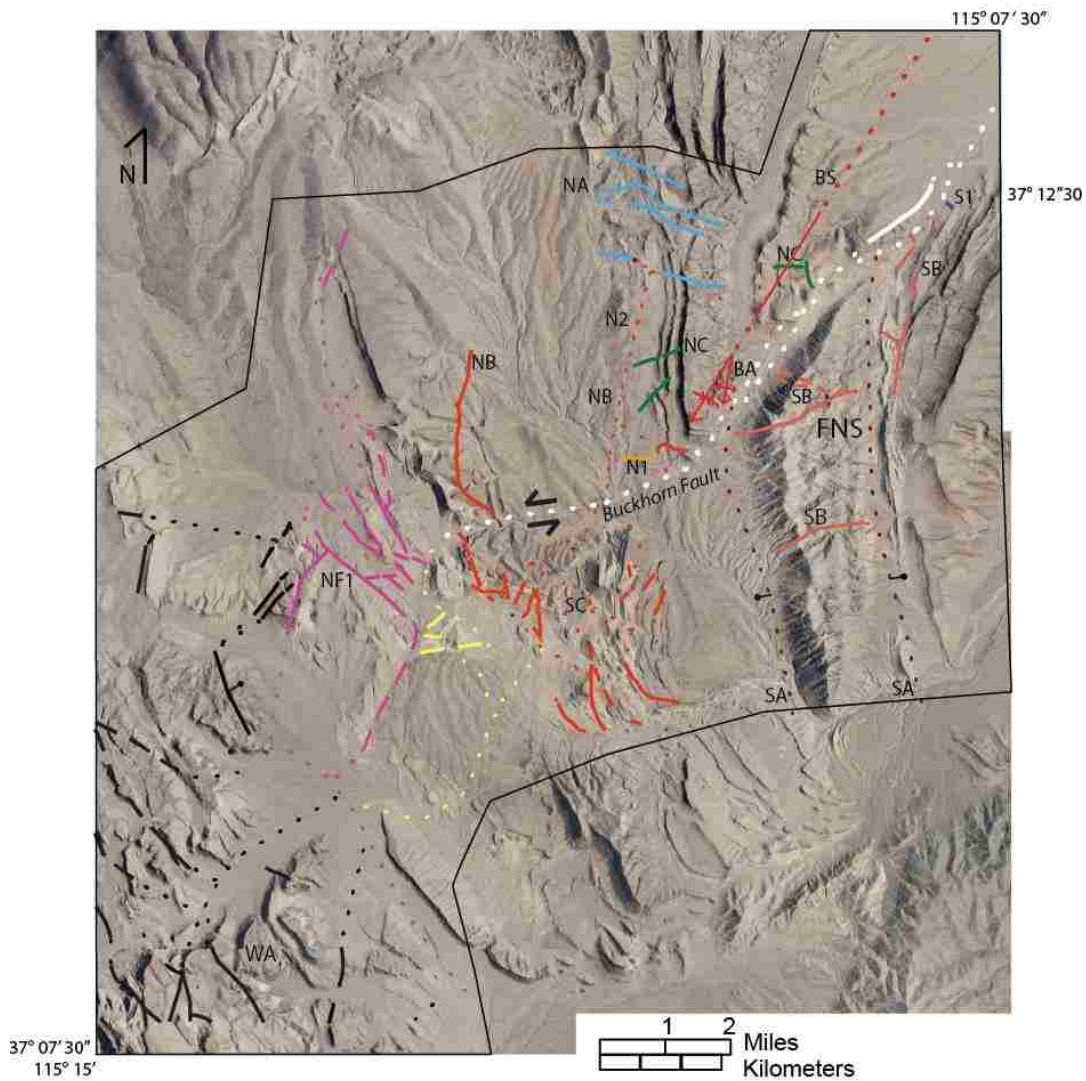
Figure 4. Fault sets and networks represented in different colors based on their interpreted association(s), or lack thereof, with the Buckhorn Fault (BF). White – BF; Red(s) – faults transferring strain onto the BF and splay faults, includes fault sets N1, NB, and SA, and fault networks SB and SC; Blue – east-west striking faults with apparent oblique slip, fault set NA; Purple – a normal fault and its associated faults into which the BF terminates, fault NF1; Yellow – set of faults that could either be associated with the BF or the normal fault (purple set); Black – faults distinct from the BF or normal fault (purple) orientation and offset; Green – faults related to the Buckhorn Syncline, fault set NC. FNS – fault network south includes both fault network SB and fault set SA. Bold black outline marks the study area. Background is composed of a set of combined orthoimages from the USGS Earth Explorer database (1997).
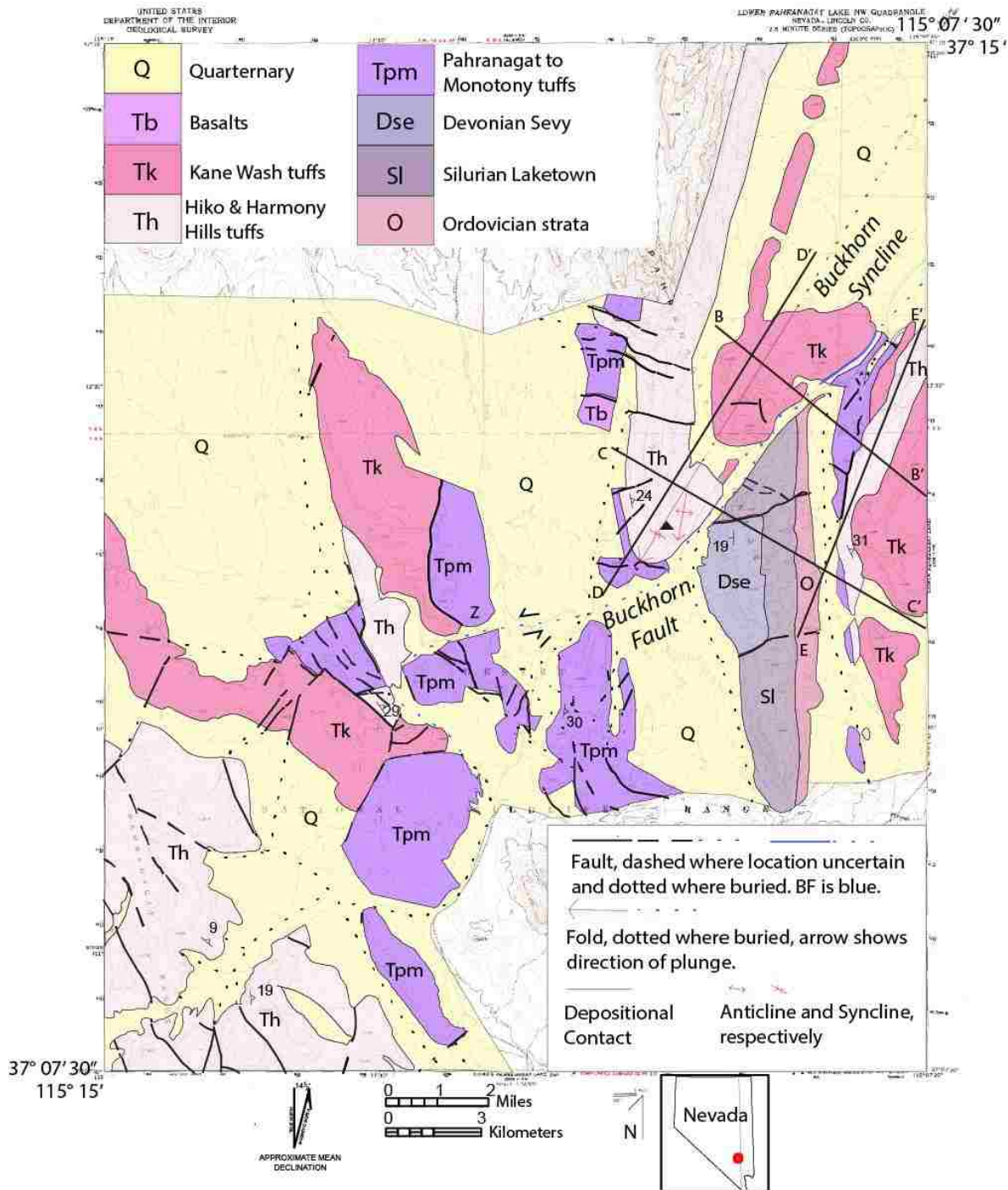
Figure 5. Simplified geologic map of study area showing general relationships among faults, folds and stratigraphy: Q – Quaternary units, Tb – Tertiary basalts, Tk – Kane Wash Tuff, Th – Miocene Harmony Hills and Hiko tuffs, Tpm – Oligocene-Miocene tuffs older than Harmony Hills, Dse – Devonian Sevy Dolomite, Sl – Silurian Laketown Dolomite, O – Ordovician Ely Springs Limestone and Eureka Quartzite. Black triangle marks location of figure 8.
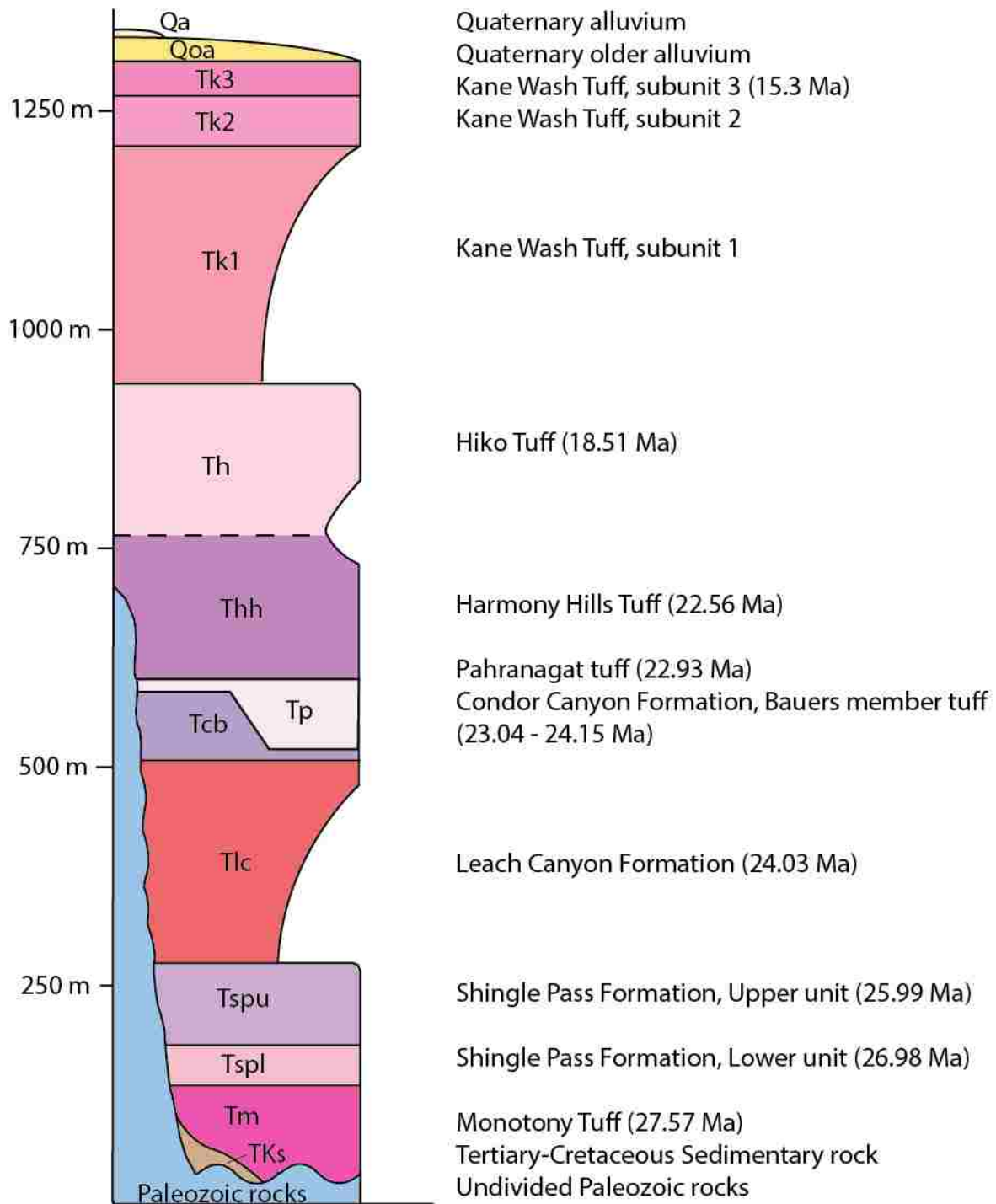
Figure 6. Stratigraphic column showing the thicknesses, calculated using thickness equations, and age relationships of the units north of the BF. For the tuffs, the right-side profile indicates degree of welding with more welded zones extending farther right. Cenozoic ages are from Best et al. (2013a, b.).
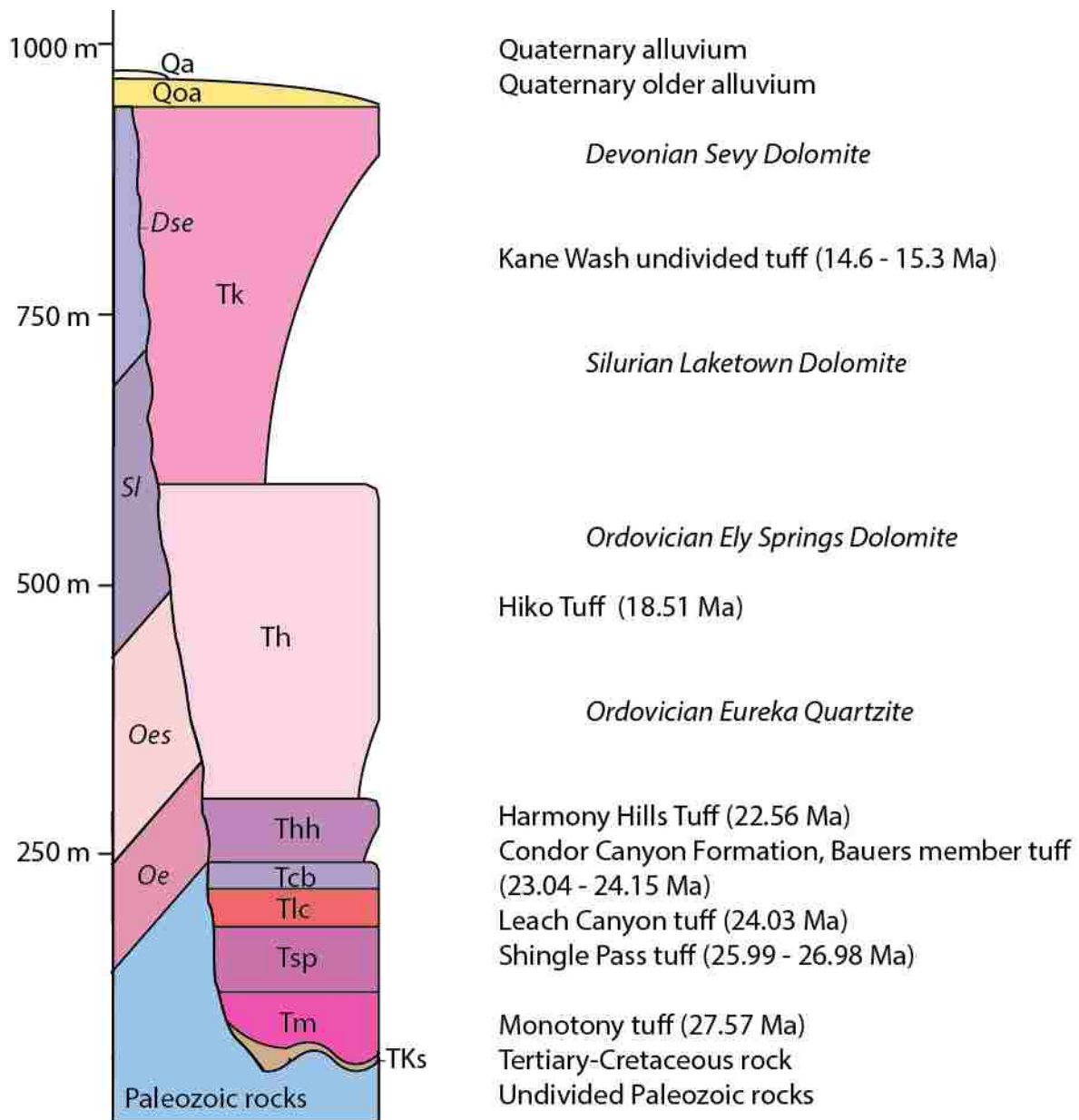
Figure 7. Stratigraphic column showing the thicknesses, calculated using thickness equations, and age relationships of the stratigraphy south of the BF. For the tuffs, the right-side profile indicates degree of welding with more welded zones extending farther right. Cenozoic ages are from Best et al. (2013a, b.).

Figure 8. Photograph looking NE approximately down the axial surface of the Buckhorn Syncline. Tkw2 and Tkw1 are two sub-units of the Kane Wash Tuff. The Buckhorn Fault (BF) is highlighted in white. Location of photographer is on figure 5.
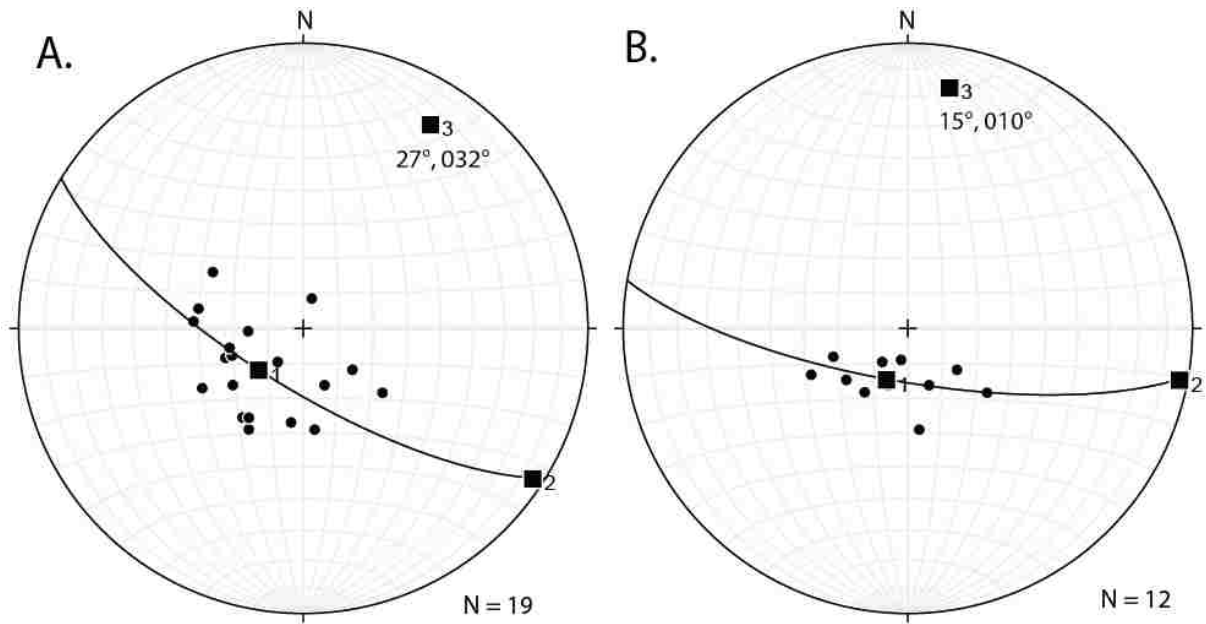
Figure 9. Stereoplots of both the (A) Buckhorn Syncline (27°, 032°) and (B) Buckhorn Anticline (15°, 010°) respectively, showing the plunge and trend of the folds and poles of the measured strikes and dips. Stereographs were plotted using Rick Allmendinger's Steronet 9 (2015).
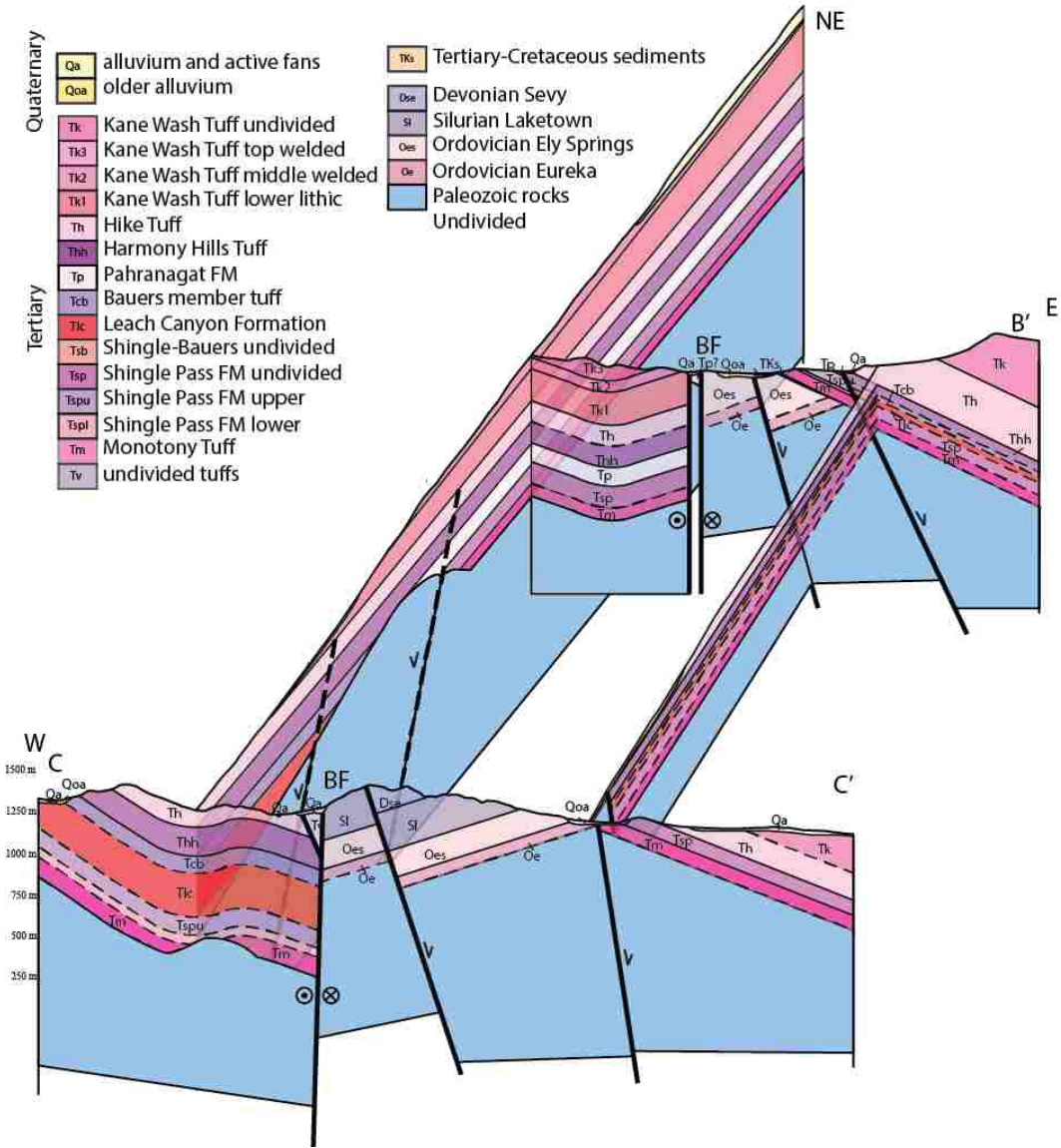
Figure 10. Fence diagram showing the geometric relationship between the BF, Buckhorn Syncline, Buckhorn Anticline, and the nearby normal faults.
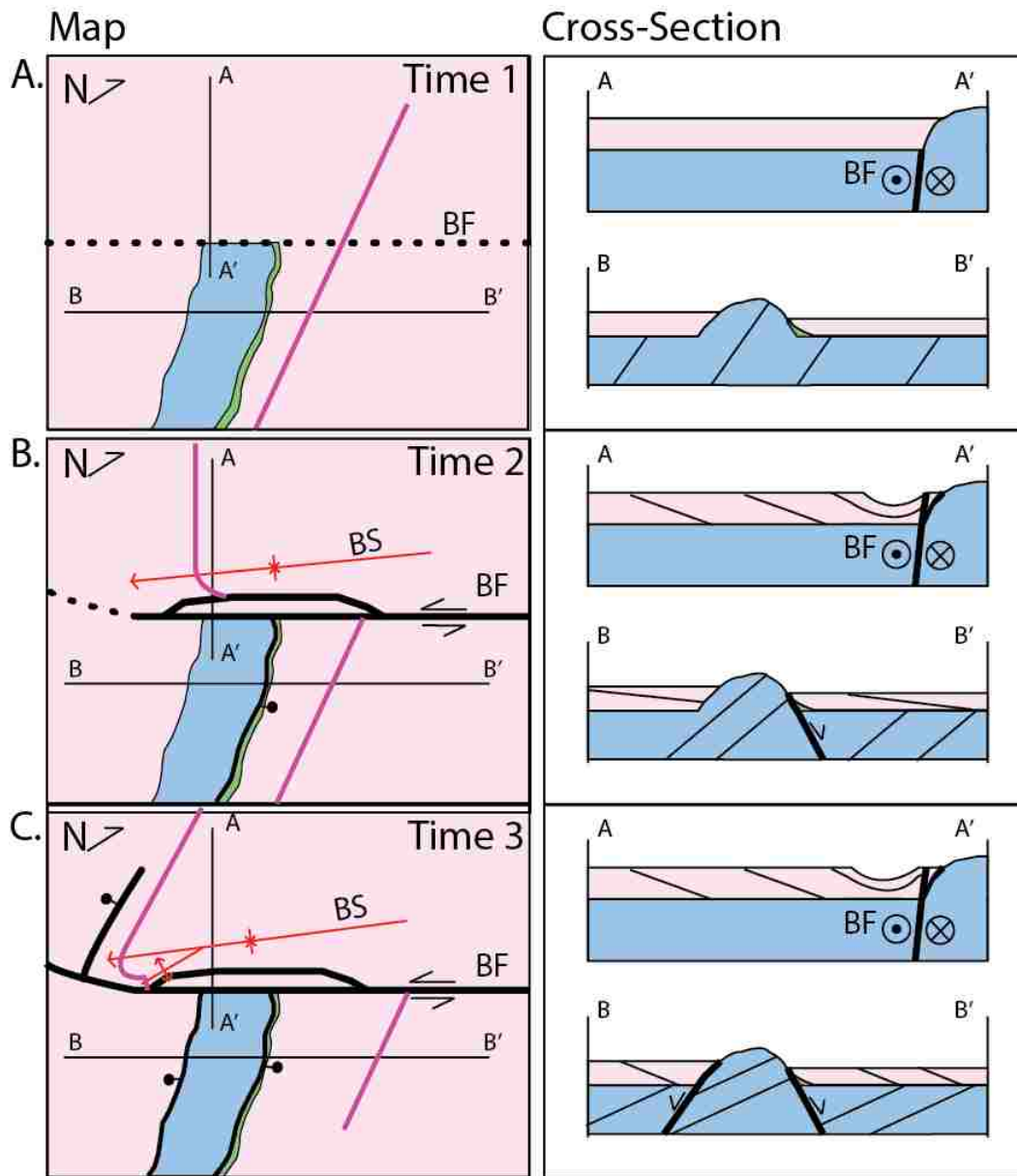
Figure 11. Diagrammatic map and cross-sections showing time-step interpretations of the evolving dip angles of beds, Paleogene unconformity, development of the Buckhorn Syncline (BS) and Anticline (BA), and propagation of the BF. Stratigraphy: Paleozoic (blue), Cretaceous to Tertiary Sediment (yellow) and Tertiary tuffs (pink). (A) Time 1 – pre-Tertiary extension. The BF before it propagates through the Tertiary tuffs, the Paleogene unconformity and the relatively steep (60° W) Paleozoic stratigraphy. (B) Time 2. The BF propagates through the Tertiary tuffs forming a fault propagation fold, the BS, the development of some normal faults, a lens forms, and the 15° E tilting of tuffs and related dip decrease of Paleozoic rocks (45° W). (C) Time 3. Continued westward propagation of the BF, development of a normal fault north of the BF, creating a contractional wedge, and the continued tilting of tuffs to 30° E and back-tilting of Paleozoic rocks to 30° W. Also, the BA develops at this time, refolding the BS south limb. Purple line acts as a marker bed to show offset through time.

41
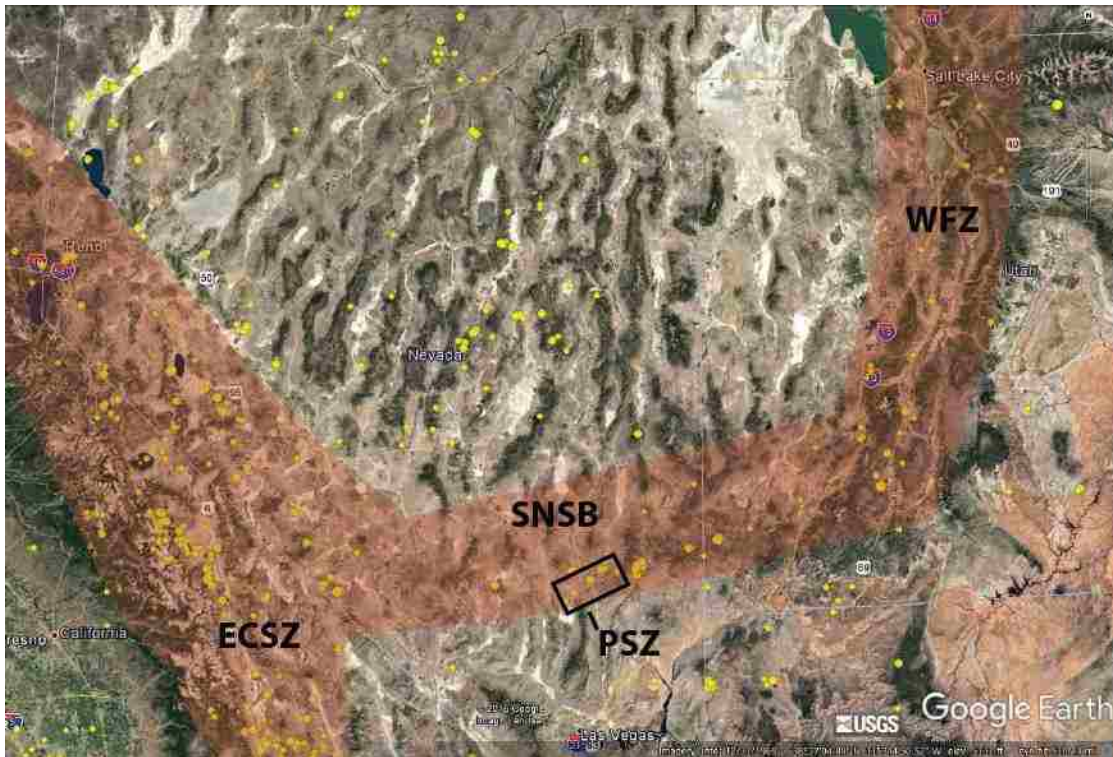
Figure 12. USGS earthquake data from 2014 to 2015 of the SW United States (USGS, 2017).
ECSZ – Eastern California Shear Zone, SNSB – Southern Nevada Seismic Belt, WFZ –
Wasatch Fault Zone. Yellow circles show locations of epicenters. Seismic zones from
Kreemer et al. (2010), and dePolo and dePolo (2012).

APPENDICES

APPENDIX A

PLATES

Plate 1. Geologic Map of the Western Buckhorn Fault, Lower Pahranagat Lake NW 7.5'
Quadrangle, Lincoln County, Nevada. (Please find the attachment entitled Geologic Map of
the Western BF)

Plate 2. Geologic cross-sections of the Western Buckhorn Fault zone. (Please find Plate 2 in the attachment entitled Geologic Cross-sections of the Western BF)

APPENDIX B

POINT COUNT and FOLD DATA

Table 1. Table containing point count statistics for sample PSZ 1-15-JB of the TK3 Tuff.

Quartz	Sanidine	Clinopyroxene	Opaques	other	matrix	total
72	161	20	5	18	968	1244
26%	58%	7%	1-2%	6-7%	22% Phenocrysts	

POINT COUNT AND FOLD DATA

Table 2. Table containing Buckhorn Syncline and Anticline attitudes.

Buckhorn Syncline	Strike	Dip	Dip Quad
1	011	31	E
2	004	32	E
3	330	34	E
4	032	31	E
5	340	24	E
6	299	33	N
7	220	18	W
8	219	28	W
9	305	31	N
10	358	16	E
11	302	30	N
12	322	26	E
13	340	22	E
14	278	27	N
15	346	22	E
16	309	12	N
17	104	09	S
18	264	29	N
19	250	17	N
Buckhorn Anticline			
1	309	12	N
2	284	09	N
3	305	22	N
4	340	23	E
5	335	31	E
6	340	23	E
7	321	23	E
8	290	17	N
9	264	29	N
10	250	17	N
11	219	29	W
12	220	18	W

GEOCHRONOLOGY

Table 3. Table showing data from NIGL on the Kane Wash 3 tuff. Temperature is 1600° C and time is one minute for all runs.

Fusion	^{36}Ar	^{37}Ar	^{38}Ar	^{39}Ar	^{40}Ar	%^{40}Ar*	Ca/K	^{40}Ar*/^{39}Ar K	Age (Ma)	1s.d.
1	0.037	0.105	0.067	4.163	23.895	83.6	0.176527	4.3838	13.65	0.66
2	0.032	0.075	0.086	5.686	31.238	92.5	0.0923148	4.7402	14.75	0.33
3	0.025	0.070	0.041	2.725	15.609	98.2	0.1797877	4.8912	15.22	0.69
4	0.038	0.093	0.172	11.973	63.046	92.7	0.0543616	4.7153	14.67	0.17
5	0.037	0.113	0.166	10.264	52.864	92.1	0.0770507	4.5515	14.17	0.19
6	0.021	0.131	0.151	11.610	61.150	98.6	0.0789686	5.0074	15.58	0.16
7	0.035	0.107	0.095	5.878	32.832	89.9	0.1274019	4.7031	14.64	0.57
8	0.028	0.083	0.126	9.608	53.165	97.5	0.0604586	5.1776	16.11	0.39
9	0.045	0.136	0.217	14.893	81.059	91.5	0.0639102	4.8447	15.08	0.15
10	0.036	0.119	0.115	7.950	44.098	88.3	0.1047607	4.7789	14.87	0.16
11	0.033	0.013	0.179	12.930	71.070	93.6	0.0071988	5.0607	15.74	0.11
12	0.030	0.072	0.109	7.707	42.353	92.2	0.0653823	4.9364	15.36	0.20
13	0.035	0.092	0.062	4.381	27.030	82.7	0.1469734	4.9096	15.28	0.07
14	0.044	0.106	0.166	10.410	60.692	87.3	0.0712639	4.9948	15.54	0.28
note: isotope beams in mV rlsd = released, error in age includes J error, all errors 1 sigma							Mean ± s.d. =		15.05	0.65
(^{36}Ar through ^{40}Ar are measured beam intensities, corrected for decay in age calculations)							Mean ± s.d. =		15.28	0.45
							(9 fusions)			
							Wtd mean age =		15.30	0.09
							(9 fusions)			
							No isochron			

GEOCHRONOLOGY PROCEDURES

Provided by NIGL lab and Dr. Terry Spell

Nevada Isotope Geochronology Laboratory - Description and Procedures

Samples analyzed by the $^{40}Ar/^{39}Ar$ method at the University of Nevada Las Vegas were wrapped in Al foil and stacked in 6 mm inside diameter sealed fused silica tubes. Individual packets averaged 2 mm thick and neutron fluence monitors (FC-2, Fish Canyon Tuff sanidine) were placed every 5-10 mm along the tube. Synthetic K-glass and optical grade CaF_2 were included in the irradiation packages to monitor neutron induced argon interferences from K and Ca. Loaded tubes were packed in an Al container for irradiation. Samples irradiated at the U. S. Geological Survey TRIGA Reactor, Denver, CO were in-core for 7 hours in the 1 MW TRIGA type reactor. Correction factors for interfering neutron reactions on K and Ca were determined by repeated analysis of K-glass and CaF_2 fragments. Measured $(^{40}Ar/^{39}Ar)_K$ values were 7.14 ($\pm$ 4.18%) x 10^{-2}. Ca correction factors were $(^{36}Ar/^{37}Ar)_{Ca} = 2.59$ ($\pm$ 1.17%) x 10^{-4} and $(^{39}Ar/^{37}Ar)_{Ca} = 8.26$ ($\pm$ 0.53) x 10^{-4}. J factors were determined by fusion of 5-6 individual crystals of neutron fluence monitors which gave reproducibility's of 0.09% to 0.12% at each standard position. Variation in neutron fluence along the 100 mm length of the irradiation tubes was <4%. Matlab curve fit was used to determine J and uncertainty in J at each standard position. No significant neutron fluence gradients were present within individual packets of crystals as indicated by the excellent reproducibility of the single crystal fluence monitor fusions.

Irradiated FC-2 sanidine standards together with CaF_2 and K-glass fragments were placed in a Cu sample tray in a high vacuum extraction line and were fused using a 20 W CO_2 laser. Sample viewing during laser fusion was by a video camera system and positioning was via a

motorized sample stage. Samples analyzed by the furnace step heating method utilized a

double vacuum resistance furnace similar to the Staudacher et al. (1978) design. Reactive

gases were removed by three GP-50 SAES getters prior to being admitted to a MAP 215-50

mass spectrometer by expansion. The relative volumes of the extraction line and mass

spectrometer allow 80% of the gas to be admitted to the mass spectrometer for laser fusion

analyses and 76% for furnace heating analyses. Peak intensities were measured using a

Balzers electron multiplier by peak hopping through 7 cycles; initial peak heights were

determined by linear regression to the time of gas admission. Mass spectrometer

discrimination and sensitivity was monitored by repeated analysis of atmospheric argon

aliquots from an on-line pipette system. Measured $^{40}Ar/^{36}Ar$ ratios were $297.37 \pm 0.05\%$

during this work, thus a discrimination correction of 0.9937 (4 AMU) was applied to

measured isotope ratios. The sensitivity of the mass spectrometer was ~6 x 10^{-17} mol mV^{-1}

with the multiplier operated at a gain of 36 over the Faraday. Line blanks averaged 1.68 mV

for mass 40 and 0.01 mV for mass 36 for laser fusion analyses and 18.34 mV for mass 40 and

0.06 mV for mass 36 for furnace heating analyses. Discrimination, sensitivity, and blanks

were relatively constant over the period of data collection. Computer automated operation of

the sample stage, laser, extraction line and mass spectrometer as well as final data reduction

and age calculations were done using LabSPEC software written by B. Idleman (Lehigh

University). An age of 28.02 Ma (Renne et al., 1998) was used for the Fish Canyon Tuff

sanidine fluence monitor in calculating ages for samples.

For $^{40}Ar/^{39}Ar$ analyses a plateau segment consists of 3 or more contiguous gas fractions

having analytically indistinguishable ages (i.e. all plateau steps overlap in age at $\pm 2\sigma$

analytical error) and comprising a significant portion of the total gas released (typically

>50%). Total gas (integrated) ages are calculated by weighting by the amount of ^{39}Ar

released, whereas plateau ages are weighted by the inverse of the variance. For each sample

inverse isochron diagrams are examined to check for the effects of excess argon. Reliable

isochrons are based on the MSWD criteria of Wendt and Carl (1991) and, as for plateaus,

must comprise contiguous steps and a significant fraction of the total gas released. All

analytical data are reported at the confidence level of 1σ (standard deviation).

REFERENCES

Allmendinger, R.W., 2015, Stereonet for Windows, v. 9, copyrighted software, http://www.geo.cornell.edu/geology/faculty/RWA/programs/stereonet.html.

Axen, G.J, 1998, The Caliente Enterprise Zone, southeastern Nevada and southwestern Utah, *in* Faulds, J.E., and Stewart, J.H., eds., Accommodation Zones and Transfer Zones: The Regional Segmentation of the Basin and Range Province: Boulder, Colorado, Geological Society of America Special Paper 323, p. 181-194.

Becker, A., 1995, Conical drag folds as kinematic indicators for strike-slip fault motion: Journal of Structural Geology, v. 17, p. 1497-1506.

Best, M.G., Anderson, R.E., Swadley, W.C., Rowley, P.D., Scott, R.B., Gromme, C.S., Harding, A.E., Deino, A.L., Sullivan, K.R., Tingery, D.G., and Christiansen, E.H., 1993, Oligocene-Miocene Caldera Complexes, Ash-flow Sheets, and Tectonism in the Central and Southeastern Great Basin: Geological Society of America Guidebook, Department of Geological Sciences, University of Nevada, Reno, p. 285-311.

Best, M.G., Gromme, S., Deino, A. L., Christiansen, E H., Hart, G. L. and Tingey, D. G., 2013a, The 36–18 Ma Central Nevada ignimbrite field and calderas, Great Basin, USA: Multicyclic super-eruptions: Geosphere, v. 9, p. 1562-1636.

Best, M.G., Gromme, S., Deino, A. L., Christiansen, E H., Hart, G. L. and Tingey, D. G., 2013b, The 36–18 Ma Indian Peak–Caliente ignimbrite field and calderas, southeastern Great Basin, USA: Multicyclic super-eruptions: Geosphere, v. 9, p. 864-950.

Bidgoli, T.S., Stockli, D.F., and Walker, J.D., 2015, Low-temperature thermochronologic constraints on the kinematic histories of the Castle Cliffs, Tule Springs, and Mormon Peak detachments, southwestern Utah and southeastern Nevada: Geosphere, v. 11, p. 850–867.

Burchfiel, B.C., 1965, Structural Geology of the Specter Range Quadrangle, Nevada, and its Regional Significance: Geological Society of America, Bulletin p. 175-192

Colgan, J. P., Dumitru, T. A., Reiners, P. W., Wooden, J. I., Miller, E.I., 2006, Cenozoic Tectonic Evolution of the Basin and Range Province in Northwestern Nevada: American Journal of Science, v. 306, p. 616-654.

DeCelles, P. G., and Coogan, J. C., 2006, Regional structure and kinematic history of the Sevier fold-and-thrust belt, central Utah: Geological Society of America, Bulletin, v. 118, p. 841-864.

DePolo, D. M., and dePolo, C. M., 2012, Earthquakes in Nevada 1840s to 2010, Nevada
    Seismological Laboratory and Nevada Bureau of Mines and Geology, Map 179.

Dickinson, W.R., 2004, Evolution of the North American Cordillera: Annual Reviews Earth
    and Planetary Science, v. 32, p. 13-45.

Dickinson, W.R., 2006, Geotectonic evolution of the Great Basin: Geosphere, v. 2, p. 353–
    368, doi: 10.1130/GES00054.1.

Duebendorfer, E.M., Sewall, A.J., and Smith, E.I., 1990, The Saddle Island detachment system;
    An evolving shear zone in the Lake Mead area, Nevada, *in* Wernicke, B.P., ed., Basin
    and Range Extensional Tectonics Near the Latitude of Las Vegas, Nevada, Geological
    Society of America Memoir 176, p. 77-97.

Dutch, S., 2014, Bouguer Gravity Anomaly Map: Gravity and Magnetic Maps of Nevada,
    University of Wisconsin, Green Bay, unofficial,
    uwgb.edu/dutchs/StateGeophMaps/NevGphMap.HTM, last accessed 11/22/2017.

Ebanks, W.J., 1965, Structural Geology of the Gass Peak Area Las Vegas Range, Nevada: Rice
    University, p. 1-56.

Faulds, J.E., and Varga, R.J., 1998, The role of accommodation zones and transfer zones in the
    regional segmentation of extended terranes, *in* Faulds, J.E., and Stewart, J.H., eds.,
    Accommodation Zones and Transfer Zones: The Regional Segmentation of the Basin
    and Range Province: Boulder, Colorado, Geological Society of America Special Paper
    323, p. 1-45.

Gawthorpe, R.L., and Hurst, J.M., 1993, Transfer zones in extensional basins: their structural
    style and influence on drainage development and stratigraphy: Journal of the Geological
    Society, London, v. 150, p. 1137-1152.

Graseman, B., Martel, S., and Passchier, C., 2005, Reverse and normal drag along a fault:
    Journal of Structural Geology, v. 27, p. 999-1010.

Guth, P. L., 1980, Geology of the Sheep Range Clack County, Nevada: Ph.D. dissertation,
    Massachusetts Institute of Technology, 193 pp.

Harding T.P., 1976, Tectonic significance and hydrocarbon trapping consequences of
    sequential folding synchronous with San Andreas faulting, San Joaquin Valley.
    California: American Association of Petroleum Geologists Bulletin, v. 60, p. 356-378.

Hudson, M.R., Rosenbaum, J.G., Gromme, C.S., Scott, R.B., and Rowley, P.D., 1998,
    Paleomagnetic evidence for counterclockwise rotation in a broad sinistral shear zone,
    Basin and Range province, southeastern Nevada and southwestern Utah: Geological
    Society of America Special Paper 323, p. 149–180.

Jayko, A. S., 1990, Shallow crustal deformation in the Pahranagat area, southern Nevada: Geological Society of America Memoir 176, p. 213-236.

Jayko, A. S., 2007, Geologic map of the Pahranagat Range Quadrangle, Lincoln and Nye Counties, Nevada: U.S. Geologic Survey, scale 1:100,000.

Kreemer, C., Blewitt, G., and Hammond, W.C., 2010, Evidence for an active shear zone in southern Nevada linking the Wasatch fault to the Eastern California shear zone: Geology, v. 38, p. 475-478.

Kreemer, C., Hammond, W.C., Blewitt, G., Holland, A.A., and Bennett, R.A., 2012, A Geodetic strain rate model for the Pacific-North American Plate boundary, Western United States: Nevada Bureau of Mines and Geology Map 178, scale 1:500,000.

Lamb, M., Beard, L. S., Hickson, T., Umhoefer, P. J., Dunbar, N., et al., 2015, Late Oligocene-early Miocene landscape evolution of the Lake Mead region during the transition from Sevier contraction to Basin and Range extension: Geological Society of America Bulletin 127. 7-8 p. 899-925.

Long, S., 2012, Magnitudes and spatial patterns of erosional exhumation in the Sevier hinterland, eastern Nevada and western Utah, USA: Insights from a Paleogene paleogeologic map: Geosphere, v. 8, p. 881-901.

Morley, C.K., Nelson, R.A., Patton, T.L., and Munn, S.G., 1990, Transfer zones in the East African rift system and their relevance to hydrocarbon exploration in rifts: American Association of Petroleum Geologists Bulletin, v. 74, p. 1234-1253.

Muhammad, M.M., 2016, Structural Evolution of the Maynard Lake Fault within the Left-Lateral Pahranagat shear zone, Nevada, USA: UNLV Thesis, Dissertations, Professional Papers, and Capstones 2798, p. 1-79, 2 plates.

O'Leary, 2000, Tectonic Significance of the Rock Valley Fault Zone, Nevada Test Site *in* Whitney, J.W., Keefer, W.R., eds, Geologic and Geophysical Characterization Studies of Yucca Mountain, Nevada, A Potential High-Level Radioactive-Waste repository: United States Geologic Survey, –Digital Dsta Series 058, paper I, p. 1-13.

Page, W.R., Swadley, W.C., and Scott, R.B., 1990, Preliminary geologic map of the Delamar 3 SW quadrangle, Lincoln County, Nevada: U. S. Geological Survey OF-90-336, scale 1:24,000.

Peacock, D.C.P., 2002, Propagation, interaction and linkage in normal fault systems: Earth Science Reviews 58, p. 121-142.

Peacock, D.C.P., Nixon, C.W., Rotevatn, A., Sanderson, D.J., and Zuluaga, L.F., 2016, Glossary of fault and other fracture networks: Journal of Structural Geology, v. 92, p. 12-29.

Price, T., Evans, M., Mahammad, M., Hinson, M., McIntyre, A., Peck, A., Taylor, W. J., 2017, Preliminary Geologic Map of the Lower Pahranagat Lake NW 7.5' Quadrangle, Lincoln County, Nevada: Nevada Bureau of Mines and Geology Open-File Report, scale 1:24000.

Rau C. J., and Forsyth D. W., 2011, Melt in the mantle beneath the amagmatic zone, southern Nevada: Geology, v. 39, p. 975-978.

Renne, P.R., Swisher, C.C, Deino, A.L., Karner, D.B., Owens, T.L., and DePaolo, D.J., 1998, Intercalibration of standards, absolute ages and uncertainties in $^{40}Ar/^{39}Ar$ dating: Chemical Geology, v. 145, p. 117-152.

Reso, A., 1963, Composite columnar section of exposed Paleozoic and Cenozoic rocks in the Pahranagat Range, Lincoln County, Nevada: Geological Society of America Bulletin, v. 74, p. 901–918.

Schlische, R.W., and Withjack, M.O., 2009, Origin of fault domains and fault-domain boundaries (transfer zones and accommodation zones) in extensional provinces: Results of random nucleation and self-organized fault growth: Journal of Structural Geology, v. 31, p. 910-925.

Scott, R. B., Page, W. R., Swadley, W. C., 1990, Preliminary geologic map of the Delmar 3 NW quadrangle, Lincoln County, Nevada: U.S. Geological Survey Open-file report 90-405, scale1:24,000.

Sonder, L.J., and Jones, C.H., 1999, Western United States Extension: How the West was Widened: Annual, Reviews, Earth and Planetary Science, v. 27, p.417–462.

Staudacher, T.H., Jessberger, E.K., Dorflinger, D., and Kiko, J., 1978, A refined ultrahigh-vacuum furnace for rare gas analysis, J. Phys. E: Sci. Instrum., 11, p. 781-784.

Swadley, W. C., Page, W. R., Scott, R.B., and Pampeyan, E. H., 1994, Geologic map of the Delamar 3 SE quadrangle, Lincoln County, Nevada: U. S. Geological Survey GQ-1754, scale 1:24,000.

Sylvester, A.G., 1988, Strike-slip faults: Geological Society of America Bulletin, v. 100, p. 1666–1703.

Taylor, W.J., Bartley, J.M., Martin, M.W., Geissman, J.W., Walker, J.D., Armstrong, P.A., and Fryxell, J.E., 2000, Relations between hinterland and foreland shortening: Sevier orogeny, central North American Cordillera: Tectonics, v. 19, p. 1124-1143.

Taylor, W. J., and Switzer, D.D., 2001, Temporal changes in fault strike (to 90°) and extension directions during multiple episodes of extension: An example from eastern Nevada: Geological Society of America Bulletin, v. 113, p. 743–759.

Tschanz, C.M., and Pampeyan, E.H., 1970, Geology and Mineral Deposits of Lincoln County, Nevada: Nevada Bureau of Mines and Geology, Bulletin 73, p. 1-187.

Umhoefer, P.J., Beard, S. L., Martin, K.L., and Blythe, N., 2010, From detachment to transtensional faulting: A model for the Lake Mead extensional domain based on new ages and correlation of subbasins *in* Umhoefer, P.J., Beard, S.L., Lamb, M.A., eds, Miocene Tectonics of the Lake Mead Region, Central Basin and Range, 2010: Geological Society of America Special Paper 463, p. 371-394.

United States Geologic Survey, 2017, Earthquake Catalog, USGS Earthquake Hazards Program 2014 to 2015 data, https://earthquake.usgs.gov/earthquakes/search/.

Van der Plas, L., and Tobi, A. C., 1965, A Chart for Judging the Reliability of Point Counting Results: American Journal of Science, v. 263, p. 87-90.

Walker, C. D., Anders, M. H., and Christie-Blick, N., 2007, Kinematic evidence for downdip movement on the Mormon Peak detachment: Geology, v. 35, p. 259-262, doi: 10.1130/G23396A.1.

Wendt, I., and Carl, C., 1991, The statistical distribution of the mean squared weighted deviation: Chemical Geology, v. 86, p. 275-285.

Zoback, M. Lou, Anderson, R.E., and Thompson, G.A., 1981, Cainozoic evolution of the state of stress and style of tectonism of the Basin and Range province of the western United States: Philosophical Transactions of the Royal Society of London. Series A, Mathematical and Physical Sciences, v. 300, p. 407–434, doi: 10.1098/rsta.1981.0073.

CURRICULUM VITAE

Thomas G. Price
8220 Cantura Peak St. (702) 682-3692 osalith@gmail.com

Education

- Bachelor of Science in Geoscience (UNLV), GPA: 3.4 (2013)
- Master of Science degree in Geoscience, with a focus in structural geology GPA: 3.8 (2017)

Abstracts with Presentations

- Price, T. G. and Taylor, W. J., 2015 Oligocene-Miocene Folded Tuffs along theBuckhorn Fault, Pahranagat Shear Zone, Nevada: UNLV Geosymposium, UNLV publication; poster presentation.
- Price, T. G. and Taylor, W. J., 2017, Mioncene-Pliocene (?) folds and normal faults associated with the left-lateral Buckhorn Fault, Pahranagat Shear Zone, Nevada: UNLV Geosymposium, UNLV publication; poster presentation.
- Price, T. G. and Taylor, W. J., 2016, Investigating Oligocene-Miocene folded tuffs and extensional faults along the Buckhorn Fault, Pahranagat Shear Zone, Nevada: Geological Society of America Abstracts with Programs. Vol. 48, No. 4, doi: 10.1130/abs/2016CD-274493; poster presentation.
- Price, T. G. and Taylor, W.J., 2017, Miocene-Pliocene (?) Folds and the left-lateral Buckhorn Fault with regional implications, Pahranagat Shear Zone, Nevada: Geological Society of America Abstracts with Programs. Vol. 49, No. 6, doi: 10.1130/abs/2017AM-305503; poster presentation.
- Price, T. G., Taylor, W. J., 2016, Miocene-Pliocene(?) folds and normal faults associated with the left-lateral Buckhorn Fault, Pahranagat Shear Zone, Nevada: AAPG Datapages/Search and Discovery Article #90266 © 2016 AAPG Pacific Section and Rocky Mountain Section Joint Meeting, Las Vegas, Nevada, October 2-5, 2016; oral presentation.

Professional Societies

- Member of AAPG student chapter 2014-2017, Vice President in 2016
- Student Member of Geologic Society of America

Work Experience

- Mineral Separation at UNLV (2012-2013)
- Teaching Assistant at UNLV (Geography, GIS, and Structural Geology) (2014-2017)
- Data Entry and Well Data, 3D drafting (summer 2017-fall 2017)

Skills and Software proficiencies

Geologic mapping, GIS, geologic interpretation, critical thinking, and problem solving. Experience working in a team and independently, with emphasis on verbal and written communication, scientific investigation, and integration of information.
Excel, Word, Adobe Illustrator, ArcMap, Power Point, Stereonet and Rockworks

Achievements

- Field Methods geologist of the year (Undergrad, UNLV)

Reference: Wanda J. Taylor, Advisor UNLV, Wanda.taylor@unlv.edu